UNIVERSITY OF BUCHAREST
Faculty of Physics

MASTER'S THESIS

PROMPT EMISSION MODEL CALCULATION FOR $^{233}U(n_{th},f)$

Author:
Ana Matei

Supervisor:
Prof. Dr. Anabella Tudora

Bucharest

2018

Acknowledgement

The author would like to thank Prof. Dr. Andreas Oberstedt and the CHANDA project for supporting my one week participation at the experiment regarding the prompt γ-ray emission of $^{233}U(n_{th},f)$ at the VVR reactor in Budapest.

I would also like to express my appreciation and thanks to my coordinator, Prof. Dr. Anabella Tudora for accepting me under her guidance and guiding me through this interesting field of research. Thank you for encouraging, for advising me all the time, and for making me a better person.

Last, but not least, I want to thank my parents for giving me all their love and support and for my friends who were there when I needed them.

Special thanks go to my colleague Alexandru for the long helpful discussions during this period.

Table of Contents

I. Introduction

Even if the fission process was discovered 70 years ago and the first major applications issued after only a few years leaded to significant changes of the word for political, social and economical point of view, this process continues to be a challenge for scientists because of its huge complexity.

Even today, although the intensive experimental and theoretical efforts of the scientific community, important aspects regarding the deep knowledge of this fission process are not yet elucidated.

The complex fission phenomenon implies two distinctive parts, the so-called pre- and post scission stages. The pre-scission part refers to the evolution of a single nucleus undergoing fission spontaneously or induced by neutrons or other particles, along the fission path up to its scission. The other stage concerns what is happening after the scission when hundred excited nuclei – i.e. the fission fragments- are involved, with continuous distributions of different shapes, kinetic energies, excitation energies and angular momenta. These fission fragments give rice to prompt neutron and prompt gamma-ray emission.

During the last decades of the XX century the scientists have given more attention to the pre-scission stage, which was intensively studied in the frame of nuclear reactions, the fission being treated as a reaction channel in competition with the other channels of the compound nucleus mechanism (e.g. elastic and inelastic scattering, γ-capture etc.). In the last 15 years the situation was inversed, many scientists focusing their efforts on the post-scission stage, i.e. on the prompt emission in fission[*)].

The deep knowledge of the prompt emission in fission is a very important request in the international context of the sustainable development concept, which re-highlights the nuclear fission as a major solution for energy needs in the near and medium future. Many important applications such as those related to the new reactor projects (Generation IV), the transmutation of the long-life nuclear wastes, the environmental protection and the radioactive waste management, the energy sources for satellites and other devices for outer space investigations, the high power propulsion (submarines and aircraft carriers), many applications in medicine, industry and so on, are only a few areas that need a high accuracy in the knowledge of processes and nuclear fission data. For this reason the fission process is a permanent priority of research programs in the European Union and the entire world.

Many quantities characterizing the prompt neutron and γ-ray emission play a crucial role in applications. For instance the energy release in fission (Q-value), which is the highest energy known and used by humanity, the total average prompt neutron multiplicity <ν> which enters the Keff multiplication factor of nuclear reactors, the prompt fission neutron spectrum (PFNS) which is the weighting function of the fast neutron group in the multi-group

[*)] This situation is very well reflected by a famous conference of the nuclear physics field, i.e. the "International Conference on Nuclear Data for Science and Technology". Its last edition, ND-2016, held in 2016 in Brugge, Belgium, has had the largest number of participants, i.e. 500 contributions. The section devoted to fission included the largest number of papers, reflecting the importance given to the fission process, and the majority of contributions of this section referred to the prompt emission in fission.

calculation data. These quantities are basic nuclear data of the evaluated nuclear data libraries (ENDF).

Almost all nuclear reactors today in service (i.e. Generation II) as well as many other applications were designed using old evaluated nuclear data available at that time, when the knowledge of the prompt emission was poor, and rude modelings were used in the evaluation of these data. The very poor power prediction of these obsolete models was reflected in high values of the safety coefficients used in the calculation and design of nuclear energetic and propulsion systems, which have led to high costs. The development of refined models based on solid physical considerations, able to provide reliable and accurate nuclear data of the prompt emission process is reflected in the reduction up to half of the total costs of new generations of nuclear reactors concomitantly with a considerable increase of their safety.

Consequently many quantities characterizing the prompt emission process whose knowledge is needed for both the application purpose and for elucidating still unclear aspects are of great interest and are research priorities at the international level, being important requirements of the Nuclear Data Section of IAEA (International Atomic Energy Agency) and of the Nuclear Energy Agency of OECD.

Important quantities characterizing the prompt emission in fission are the prompt neutron multiplicity and prompt γ-ray energy as a function of fragment mass (A), charge (Z) and total kinetic energy (TKE), the total average prompt neutron multiplicity and spectra, the prompt γ-ray energy, multiplicity and spectra as a function of incident neutron energy (En), the prompt neutron emission probability and so on. The concomitantly good description of these quantities by a single modeling (without adjustments of input data) assures both the consistency of an evaluation and the prediction of all prompt emission data needed in applications. This desiderate can be accomplished only by the development of refined and reliable theoretical models based on solid physical considerations. New experiments to provide accurate experimental information about different prompt emission quantities and for many actinides are welcome being needed for the validation of developed modelings.

I.1 Present status of the modeling of prompt emission in fission

In the last decade remarkable efforts were done in the development of prompt emission models. The comprehensive paper [Capote et al., 2016] includes a short description of the most important prompt emission models and the associated computer codes. Nowadays there are two categories of prompt emission codes including refined modelings that can provide the majority of data characterizing the prompt neutron and γ-ray emission in fission with a reasonable and/or good accuracy. They are the following

A. Computer codes with a probabilistic Monte-Carlo treatment of the sequential emission

Three computer codes are representative for this category, i.e.:

A.1. FIFRELIN: developed at Commissariat ă l"Energie Atomique (CEA) - Cadarache, France (O.Serot, O.Litaize and co-workers). The initial version of this code [Litaize and Serot, 2010] included a prompt emission simulation using a Weisskopf-Ewing spectrum. In

the recent versions the de-excitation of fission fragments is treated with the Hauser-Feshbach formalism and [Regnier et al., 2013].

A.2. CGMF: developed at Los Alamos National Laboratory, USA (P.Talou and co-workers). This code represents a merger of two codes previously developed at LANL, i.e. a code which performed Monte Carlo simulations following the Weisskopf-Ewing statistical theory [P.Talou et al., 2011] and another code including the statistical Hauser-Feshbach model [Kawano et al., 2010] which was not initially developed for treating fission events.

A.3. FREYA developed at Lawrence Livermore National Laboratory, USA (J.Randrup and R.Vogt, [Vogt and Randrup, 2014]).

These Monte Carlo codes use as input fission fragment distributions. They employ different methods and parameterizations for the TXE partition, which are based on the same physical considerations regarding the nascent fragments at scission, i.e. they are in the Fermi-gas regime of level densities and in statistical equilibrium at scission.

A semi-empirical code, which can be also included in this category, is:

A.4. GEF: developed by K.-H.Schmidt and B.Jurado. A comprehensive description of this code can be found in Ref.[Schmidt et al., 2016]. In the last years this code has become popular (especially for experimentalists) because it can be freely download and it can be used even by physicists not familiarized with the fission process due to its very simple input. A part of the physical considerations on which the GEF code is based (e.g. regarding the TXE partition) are completely different compared to all other prompt emission codes.

Unlike the three codes mentioned above, the code GEF also calculates fission fragment distributions.

B. Computer codes with a deterministic treatment of prompt emission

This category includes only two modelings and associated codes, both developed at the University of Bucharest (A.Tudora and co-workers), i.e.:

B.1 The Point-by-Point (PbP) model and computer code which takes into account multiple fragmentations of a fissioning nucleus covering the entire fragment mass and charge ranges at TKE values going from about 100 to 200 MeV. In the PbP treatment the sequential emission from each initial fragment of the fragmentation range at each TKE value is globally taken into account by a residual temperature distribution P(T) with an analytical form. Details about the PbP model can be found in Refs. [Tudora and Hambsch, 2017], [Capote et al., 2016] and references therein. Chapter II of this dissertation is devoted to the description of the PbP model.

B.2 A sequential emission treatment based on recursive equations of residual temperatures which are solved for each initial fragment of the fragmentation range at each TKE (constructed as in the PbP treatment) at each TKE. Details about this modeling are given in Ref. [Tudora et al., 2018] and [Tudora and Hambsch, 2018].

The same TXE partition based on modeling at scission is used in both deterministic modelings. The physical considerations related to scission are similar with the ones of three MC codes mentioned above (i.e. nascent fragments in statistical equilibrium at scission with level densities in the Fermi-gas regime). Both codes use fragment distributions Y(A,TKE) as input.

The models and associated codes of these two categories are able to provide all observables of interest related to fission fragments and prompt emission on an event-by-even basis, i.e. they can provide a great amount of data sliced in many subspaces, giving distributions and correlations of prompt fission neutrons and γ-rays, e.g. ν(A,Z,TKE), Eγ(A,Z,TKE), <ε>(A,Z,TKE), P(ν), ν(A), ν(TKE) etc.

C. Most probable fragmentation approach – the Los Alamos model

Apart from these modelings, the Los Alamos (LA) model deserves a special mention, too. This model takes into account only one fragmentation of the fissioning system, the so-called "most probable fragmentation approach". Consequently it provides only total average prompt emission quantities, i.e. total average prompt neutron multiplicity <ν> and spectrum (PFNS) and eventually total average prompt γ-ray energy <Eγ>[Madland and Nix, 1982].

The LA model has been the workhouse behind most of the modern PFNS data evaluations thanks to a limited number of model input parameters that can be adjusted to reproduce experimental PFNS and prompt neutron multiplicity data and that can be applied to all actinides and incident neutron energies up to 20 MeV or more[Madland and Nix, 1982].

The LA model in its initial form was proposed by [Madland and Nix, 1982]by D.G.Madland and J.R.Nix in 1982. During the time it was extensively developed. Among the most significant improvements brought to the LA model, a part being briefly discussed in Ref. [Capote et al., 2016], the following ones are mentioned here:

- The extension of the LA model at incident neutron energies higher than 20 MeV by taking into account the fission of secondary compound nuclei formed by charged particle emission. This development was done by A.Tudora and co-workers in 2004 [Tudora et al., 2004].
- The inclusion of the concept of multi-modal fission by taking into account several most probable fragmentations corresponding to each fission mode. This improvement is due to T.Ohsawa and co-workers and A.Tudora and co-workers (many references about can be found in [Capote et al., 2016]).
- The well-known fact that the prompt neutrons emission takes place at the full acceleration of fission fragments is considered in all prompt emission models. However the inclusion into the LA model of neutrons emitted during the acceleration of fragments, by T.Ohsawa and co-workers [Ohsawa et al., 2011]and [Capote et. al., 2013] leaded, in some cases, to an improvement of PFNS results.
- Non-equal maximum values of the residual temperature distribution (as in the PbP model) were recently included in the LA model by D.G. Madland himself [Madland and Kahler, 2017].
- The most recent improvement consists in the use into the LA model of another triangular form of the residual temperature distribution P(T), resulting from the sequential emission treatment based on recursive equations of residual temperatures, as proposed in Ref. [Tudora et al., 2018]. This work is in progress and the consideration of separate P(T) associated to each emission sequence is foreseen, too.

A systematic of average values of the input parameters for the LA model was also developed by A.Tudora [Tudora, 2009]. This is very useful taking into account the extensive use of this model in PFNS evaluations.

I.2 Motivation of this work

Accurate evaluated nuclear data for the neutron-induced fission of ^{233}U was and continue to be an important requirement at international level because ^{233}U is the fissile nucleus of the Th-U fuel cycle, which will be used in future energetic applications, i.e. Accelerator Driven Systems (ADS).

The recent Coordinated Research Project (CRP) of IAEA having as subject the evaluation of prompt fission neutron spectra of actinides has included the PFNS evaluation of ^{233}U, too. A comprehensive description of the works done in the frame of this project is given in Ref. [Capote et al., 2016].

The PFNS evaluation for ^{233}U(n,f) performed in the frame of this CRP was based on the PbP model treatment, which has provided the total average values of different fission fragment quantities (e.g. energy release, total kinetic energy, average neutron separation energy, level density parameter). These average values together with the systematic of Ref. [Tudora, 2009] have assured the input of the most probable fragmentation approach (LA model) which was used to provide the evaluated PFNS from thermal En up to 20 MeV. More details about can be found in Section VII.G of Ref.[Capote et al., 2016] where it is explicitly mentioned that, "the PFNS evaluation for neutron induced fission of ^{232}Th, ^{233,234}U and ^{237}Np with incident neutron energies from thermal to 20 MeV is exclusively model based" (i.e. on the PbP model and the systematic of average input parameters for the LA model [Tudora, 2009]). Because the IAEA-CRP mentioned above concerned prompt neutron spectrum evaluations, only the PFNS of ^{233}U(n_{th},f) was reported in Section IV.C of Ref. [Capote et al., 2016]. For this reason the model calculation results of other prompt emission quantities of ^{233}U(n_{th},f) are required as evaluated nuclear data for multiple applications (e.g. prompt neutron multiplicity, prompt γ-ray energy and multiplicity).

The present work answers to this requirement by reporting PbP model results of the prompt neutron and γ-ray quantities mentioned above.

During the time the prompt emission of γ-rays was less investigated than the prompt neutron emission, this fact being reflected in the scarcity of experimental data regarding the prompt γ-rays. For this reasons during the last years many experimental efforts were addressed to prompt γ-ray emission. They were materialized in accurate prompt γ-ray spectrum data of important actinides (e.g. ^{252}Cf(SF), ^{235}U(n,f), ^{239}Pu(n,f), ^{240,242}Pu(SF)) measured by a team of experimentalists from prestigious institutes. Details about these experiments can be found e.g. in Refs.[Oberstedt et al, 2018; Gatera et al., 2018; Wilson et al., 2018] and references therein).

Recently (February 2018) a team including scientists from IFIN-HH-ELI-NP, Romania, EC-JRC-Geel, Belgium, IPN-Orsay, France, has performed a first measurement campaign devoted to the prompt γ-rays of ^{233}U(n_{th},f) in the frame of the international project CHANDA. As in previous cases, the experiment has taken place at the Budapest research reactor VVR. The author of this dissertation participated at this measurement campaign, too. The processing of measured data of this experiment is in progress.

The Point-by-Point model results concerning the prompt γ-ray energy and multiplicity of ^{233}U(n_{th},f) obtained in the frame of this dissertation can be useful in the processing of experimental data mentioned above, this being a second motivation of the present work.

I.3 Structure of the present dissertation

This dissertation, having as subject the prompt emission calculation for $^{233}U(n_{th},f)$, is organised in four chapters as following.

The first chapter, i.e. this introduction, includes a short review of the importance of accurate evaluated nuclear data for fission and the actual status of prompt emission models and the associate computer codes, as well as the motivation of this work.

The second chapter is devoted to the description of the PbP model of prompt emission, which is applied on $^{233}U(n_{th},f)$ in the frame of this work.

The third chapter, entitled "Results and discussions", includes the original results of this work. This chapter is organised in several sections as follows. It stars with a section about the available experimental single distributions of fission fragments from which the multiple fission fragment distributions Y(A,Z,TKE), needed in the PbP treatment, are re-constructed. A second section is devoted to the presentation of PbP model results for many prompt emission quantities in comparison with the existing experimental data. The good description of these data by the PbP model results, starting from the multi-parametric prompt neutron multiplicity matrix ν(A,TKE), continuing with single distributions of prompt emission quantities (e.g. ν(A), ν(TKE), Eγ(A), Nγ(A) etc.) up to total average quantities (e.g. total average number of prompt neutrons and total average γ-ray energy), is the most important validation of present PbP model results. The comparison of these PbP model results with the ones provided by a recent deterministic model of sequential emission constitutes a supplementary validation. The last section of this chapter includes PbP model results of other quantities characterizing both the fission fragments and the prompt emission for which experimental data does not exist, as well as total average values of fission fragment quantities which can be used as input for the "most probable fragmentation approach" (Los Alamos model).

The last chapter includes the conclusions. Detailed prompt emission results of model calculation for the fissioning system $^{233}U(n_{th},f)$ are for the first time reported in the frame of this work. They were included in a paper recently submitted to Roum. Rep.in Physics.

The reference list follows the last chapter. The present dissertation contains also an appendix which includes ν(A,TKE) results of the sequential emission model (serving for comparison with the PbP model results of this work) and a comparison of prompt emission results obtained in this work with those provided by the GEF code.

II. A brief description of the Point-by-Point prompt emission model

The Point-by-Point (PbP) model gives, as primary results, the multi-parametric matrices of different quantities as a function of fragment mass *A*, charge number*Z* and total kinetic energy of the fission fragments (*TKE*).A complete treatment of the nuclear fission process requires an analysis in terms of all the parameters (A,Z,TKE). The PbP treatment include a large number of multi-parametric matrices associated with the relevant physical quantities (i.e. the level density parameter, a(A,Z,TKE), fragment excitation energy at full acceleration E^*(A,Z,TKE), prompt neutron multiplicity ν(A,Z,TKE), the prompt neutron spectrum *N(A,Z,TKE, E)*, the prompt gamma-ray energy E_γ*(A,Z,TKE)*.). These multi-parametric matrices are generecallylabeled as q(A,Z,TKE),([Tudora and Hambsch, 2017]and references therein). These matrices are independent of the fragment distributions *Y(A,Z,TKE)*.The model uses only data from Nuclear Data Libraries such as: mass excesses, shell corrections, optical parameterizations etc.

Single or double parameter distributions of different quantities, such as q(A), q(TKE) q(A,TKE) (e.g ν(A,TKE), E_γ(A) etc.) depend on the multiple fragment distribution Y(A,Z,TKE), being obtained by averaging the corresponding matrices q(A,Z,TKE) over this distribution. However, it is through these secondary results that PbP model can be validated.[Capote et al. 2016] and [Tudora and Hambsch, 2017].

II.1.The Fragmentation Range in Point-by-Point Treatment

For a comprehensive and relevant account for the post-scission part of the fission process, it is necessary to take into account many fragmentations covering the entire A range and a large TKE range.These fragmentations mean the so-called fragmentation range or domain which plays a crucial role in the Point-by-Point model (PbP) [Tudora and Hambsch,2017].

The fragment range is defined by the mass number A, the charge number Z and the total kinetic energy TKE. The mass number A is taken from symmetric fission up to a very asymmetric split with a step of 1 mass unit. Three or five charge numbers Z are taken into consideration for each A, as the nearest integers above and below the most probable charge Z_p.[Tudora and Hambsch,2017].

$$Z_p(A) = Z_{UCD}(A) + \Delta Z(A) \quad (1)$$

In Eq. (1) Z_{UCD} isthe unchanged charge distribution (UCD), which is defined as $Z_{UCD}^{L,H} = AZ_0/A_0$(where Z_0 and A_0 are the charge and the mass numbers of the fissioning nucleus) andΔZ(A) is the charge polarization (deviation).

Several possibilities exist regarding the charge deviations: either as a function of A or as a constant value taken for all A, i.e. ΔZ=+/- 0.5 (the plus sign for the light fragment(LF) and the minus sign for the heavy fragment(HF)). The mean ΔZ value (obtained by averaging

ΔZ (A) over Y(A)) is of about 0.5 for all studied fissioning nuclei for which ΔZ(A) and rms(A) exist (e.g. ^{233,235}U(n_{th},f), ^{234}U(n,f), ^{239}Pu(n_{th},f), ^{252}Cf(sf), $^{236\text{-}244}$Pu(SF) etc.). For each fragmentation a large TKE range is taken into account, e.g. from 100 to 200 MeV, with an usual stepsize of 5 MeV[Tudora and Hambsch,2017].

II.2. Partition of the Total Excitation Energy (TXE)

One of the most important challenges in modeling the prompt emission process is the partitioning of total excitation energy at full acceleration (TXE) between complementary fragments, i.e.$TXE = E_L^* + E_H^*$.

There are several methods forthe TXE partition that are used in different models of prompt emission, each one based upon different physical assumptions about what is happening at scission.Depending on these assumptions, partitioning takes place: a). at scission between complementary nascent fragments or b) before scission between complementary pre-nascent fragments, thus the total energy that is shared can vary considerably from one TXE partition method to another [Tudora et. al. 2015b].

The total excitation energy (TXE) of each pair of fully accelerated fragments (i. e. fragmentation) is obtained from the balance of energy:

$$TXE = E_r + E_n + B_n - TKE \tag{2}$$

whereE_r(Q-value) is the energy release of a fragment pair which is obtained from the mass excesses available in different nuclear data libraries (the most used is the database of Audi and Wapstra from in RIPL-3 [RIPL-3, 2009a]), E_n is the incident neutron energy and B_n is the neutron binding energy. In the case of spontaneous fission both En and $B_n$are taken zero.

The TXE partition method in the PbP model was first of total was first described in [Morariu et. al., 2012]. An advantage of this method is based only on data from nuclear data libraries(e.g. deformations, mass excesses etc).

The TXE partition methodof the PbP treatment is based on the following assumptions at scission[Tudora et. al. 2015b]:

a). thermodynamic/statistical equilibrium: $\tau_L = \tau_H$;

b). the level density of nascent fragments is in the Fermi-Gas regime.

Therefore the modeling of this method starts from the energy conservation at scission for a pair of nascent fragments [Ruben et. al., 1991; Marten et. al., 1989; Morariu et. al., 2012; Tudora et. al., 2015b]:

$$E_r + E_n + B_n = E_{pre} + E_{Coul} + E_{sc}^* + \Delta E_{def}^L + \Delta E_{def}^H \tag{3}$$

where E_{pre} is the pre-scission kinetic energy, $E_{Coul.}$is the Coulomb repulsion energy between the nascent fragments, $\Delta E_{def}^{L,H}$ is the extra-deformation energy of a fragment at scission compared to full acceleration andE_{sc}^* is the available excitation energy at scission. At full acceleration $TKE = E_{pre} + E_{Coul}$ and the total excitation energy of complementary fragments

become: $TXE = E_{sc}^{*} + \Delta E_{def}^{L} + \Delta E_{def}^{H} = E_{L}^{*} + E_{H}^{*}$ [Morariu et. al. 2012; Tudora et. al., 2015b].

This method includes two steps. The first step consist in the calculation of the extra-deformation energy of each fragment.[Tudora et. al., 2015b]ass difference between the absolute deformation energy of a fission fragment at scission and at full acceleration (taking into account the assumption that fragments are more deformed at scission than at full acceleration [Tudora et. al., 2015a].

The absolute energy is defied with respect to the spherical shape, using the liquid drop model (LDM)[Tudora et. al., 2015b]:

$$E_{def}\left(\beta\right) = E_{LDM}\left(\beta\right) - E_{LDM}\left(\beta = 0\right) \tag{4}$$

where: β stands for the quadrupole deformation parameter, β_2.

Consequently,the extra-deformation energy becomes:

$$\Delta E_{def}^{L,H} = E_{def}\left(\beta_{sc}\right) - E_{def}\left(\beta_{full\ acc.}\right) \tag{5}$$

Taking into account that at full acceleration the fragments are much less deformed that at scission, a good approximation is to used at full acceleration the values of β at ground state deformation (available in nuclear data libraries in Ref. [RIPL-3, 2009b]) [Tudora et. al., 2015b].

The second step consists in the subtracting the extra-deformation energies, calculated before, from TXE in order to obtainE_{sc}^{*}. Therefore we can calculate the available excitation energy at scission, as:

$$E_{sc}^{*} = TXE - (\Delta E_{def}^{L} + \Delta E_{def}^{H}) = E_{sc}^{*L} + E_{sc}^{*H} \tag{6}$$

Due to the fact that the magnitude of TXE is between 25-50 MeV for different fissioning systems at low and moderate incident neutron energy and that the extra-deformation energy does not exceed 10 MeV, the available excitation energy at scission is high enough to consider the level density in the that Fermi-Gas regime[Morariu et. al., 2012].Consequently the fragment excitation energy at scission can be express as a function of level density parameter and the nuclear temperature. By assuming statistical equilibrium at scission ($\tau_L = \tau_H = \tau$), the available excitation energy at scission is shared between the complementary nascent fragments according to the ratio [Tudora et. al., 2015b]:

$$\frac{E_{sc}^{*L}}{E_{sc}^{*H}} = \frac{a_{sc}^{L}}{a_{sc}^{H}} \tag{7}$$

where $a_{sc}^{L,H}$ are the effective level density parameters accounting for collective and intrinsic/single-particle excitations[Morariu et. al., 2012].

The level densities [Tudora and Hambsch, 2017] are usually obtained using the super-fluid model:

$$a\left(A,Z,E^{*}\right)=\begin{cases}\tilde{a}\left(\mathrm{A}\right)\left(1+\dfrac{\delta\mathrm{W}\left(\mathrm{A},\mathrm{Z}\right)}{\mathrm{U}^{*}}\left[1-\exp\left(-\gamma\left(\mathrm{A}\right)\mathrm{U}^{*}\right)\right]\right), & U^{*}=E^{*}-E_{cond}, E^{*}>E_{cr},\\ a_{\mathrm{cr}}=\tilde{a}\left(\mathrm{A}\right)\left(1+\dfrac{\delta\mathrm{W}\left(\mathrm{A},\mathrm{Z}\right)}{\mathrm{E}_{\mathrm{cr}}}\left[1-\exp\left(-\gamma\left(\mathrm{A}\right)\mathrm{E}_{\mathrm{cr}}\right)\right]\right) & E^{*}\le E_{cr,}\end{cases} \quad (8)$$

where: $E^{*}$is the excitation energy of the fragment; δW(A,Z) is the shell correction; $\mathrm{E_{cr}}$ is the critical energy when the phase transition between super-fluid and normal states takes place; the values of $\mathrm{E_{cr}}$ and $\mathrm{a_{cr}}$ are obtained through an iterative procedure and $E_{cr}=a_{cr}t_{cr}^{2};$ with the critical temperature, $\mathrm{t_{cr}}$ = 0.567Δ; the condensation energy is $E_{cond}=3a_{cr}\frac{\Delta^{2}}{2\pi^{2}}-n\Delta$ where Δ =12/$\sqrt{A}$ and is the pairing correlation function with n=0, 1, 2 (for even-even, odd-A and odd-odd nuclei).$\gamma(A)=\gamma_{0}A^{-1/3}$ is the damping of shell effects and $\tilde{a}$is the asymptotic level density parameter (washing out of shell effects)[Tudora and Hambsch, 2017].

It follows that the fragment excitation energy at full acceleration is:

$$E_{L,H}^{*}=E_{sc}^{L,H}+\Delta E_{def}^{L,H} \quad (9)$$

An interesting initial condition is given by the following pattern of the ratio $\mathrm{E^{*}_{H}/TXE}$ as a function of $\mathrm{A_H}$:for fragment pairs with $\mathrm{A_H}$less than ~140-144 this ratio is less than 0.5 with a minimum placed at $\mathrm{A_H}$ around 130 (due to the magic or double magic heavy fragment with N = 82 si Z = 50). The ratio $\mathrm{E^{*}_{H}/TXE}$ is of about 0.5 at $\mathrm{A_h}$ placed around 140 (which corresponds to the most probable fragmentation) and it exhibits an almost linear increase for $\mathrm{A_H}$ above this value. With increasing excitation energy the minimum value of this ratio at ~ 130 is increasing. The same pattern is exhibited by the neutron multiplicity, ν(A). In fact this observation, due to Wahl can be used to partition ν directly[Tudora and Hambsch,2017].

II.3. Single fragment emission in the Point-by-Point model

It is assumed that the energy spectrum of prompt neutrons in the CMS is a Weisskopf-Ewing evaporation spectrum:

$$\varphi\left(\varepsilon\right)\sim\sigma_{c}\left(\varepsilon\right)\varepsilon\ exp(-\frac{\varepsilon}{T}) \quad (10)$$

where: ε is the energy of the neutron in the center-of-mass frame, $\sigma_c(\varepsilon)$ stands for the compound nucleus cross section of the inverse process of neutron evaporation from the fragment and T is the nuclear temperature of the residual fragment[Capote et. al., 2016;Tudora and Hambsch,2017].

The compound nucleus cross sections $\sigma_c(\varepsilon)$ of all fragments are obtained by optical model calculations using the SCAT2 computer code [Bersillon, 2010] with phenomenological optical potential parameterizations appropriate for nuclei appearing as fission fragments (e.g. of Becchetti-Greenlees from RIPL 3[RIPL-3, 2009c].

To take into account the sequential emission in a global way, it is necessary to introduce a residual temperature distribution P(T)[Tudora and Hambsch,2017]. Consequently

the prompt neutron spectrum in SCM at a given T (Eq.(10)) is integrated over the P(T) distribution:

$$\Phi(\varepsilon)=\int_0^{T_{\max}}\frac{\sigma_c(\varepsilon)\varepsilon e^{\left(-\frac{\varepsilon}{T}\right)}}{\int_0^{\infty}\sigma_c(\varepsilon)\varepsilon e^{\left(-\frac{\varepsilon}{T}\right)}d\varepsilon}P(T)d\varepsilon \tag{11}$$

There are multiple choices for the residual temperature distribution P(T). The most used is the triangle form Ref.[Madland and Nix, 1988]:

$$P(T)=\begin{cases}\dfrac{2T}{T_m^2} & T\le T_m\\ 0, & T>T_m\end{cases} \tag{12}$$

In the P(T) form of Madland and Nix, the maximum temperature T_m is taken equal to the temperature of initial fragments (before the neutron emission)[Tudora and Hambsch,2017]. Considering the fully accelerated fragment in the Fermi gas regime of level density, T_m of Eq.(9) is given by:

$$T_m=\sqrt{\frac{E^*_{L,H}}{a_{L,H}}} \tag{13}$$

The prompt neutron spectrum in the laboratory frame is calculated as:

$$N(E)=\int_{\left(\sqrt{E}-\sqrt{E_f}\right)^2}^{\left(\sqrt{E}+\sqrt{E_f}\right)^2}\frac{\Phi(\varepsilon)}{4\sqrt{\varepsilon E_f}}d\varepsilon \tag{14}$$

where $\Phi(\varepsilon)$ is given by Eq. (11), E is the neutron energy in the laboratory frame and E_f is the average kinetic energy per nucleon $E_{f\,L,H}=\left(\frac{A_{H,L}}{A_{L,H}}\right)\left(\frac{TKE}{A_L+A_H}\right)$[Tudora and Hambsch, 2017].

The most important part of the prompt neutron emission takes place at full acceleration. However, evaporation during acceleration is also possible and leads to a non-isotropic spectrum in the center of mass frame. Terell assumed that the anisotropy, if it exists, is symmetrical around 90°, i.e. $\Phi(\varepsilon,\theta_{cm}) = \Phi(\varepsilon)\ (1\text{-}b\cos^2\theta_{cm})/1+b/3)$ where $\Phi(\varepsilon)$ is obtained from Eq.(11) and b is the anisotropy parameter. If we replace $\cos\theta_{cm}$ from $E=\varepsilon+E_f+2\sqrt{\varepsilon}E_f cos\theta_{cm}$ into the $\Phi(\varepsilon,\theta_{cm})$ formula, the prompt neutron spectrum in the laboratory frame becomes[Tudora and Hambsch,2017]:

$$N(E)=\int_{(\sqrt{E}-\sqrt{E_f})^2}^{(\sqrt{E}+\sqrt{E_f})^2}\frac{\Phi(\varepsilon)}{4\sqrt{\varepsilon E_f}}\frac{1+b(E-\varepsilon-E_f)^2/4(E-\varepsilon-E_f}{1+b/3}d\varepsilon \tag{15}$$

In general, the anisotropy is not taken into account in the PbP calculations (i.e. the parameterb is set to 0) because it is difficult to assign a value of b for each fragment. Moreover, in a great part of cases, the experimental spectrum data were well described by Pbp results without to consider the anisotropy[Tudora and Hambsch, 2017].

The weights of the complementary fragments can be expressed as: $r_H = \frac{E_H^*}{TXE}$, $r_L = 1 - r_H = = \frac{E_L^*}{TXE}$ and they serve to calculate different quantities associated to a fragment pair (fragmentation). For instance:N(E)= $r_L*N_L(E) + r_H*N_H(E)$, $<\varepsilon> = r_L<\varepsilon_L> + r_H<\varepsilon_H>$and $\Phi_{pair}(\varepsilon) = r_L \Phi_L(\varepsilon) + r_H \Phi_H(\varepsilon)$[Tudora and Hambsch, 2017].

Other quantities provided by the PbP model arethe energy carried away per neutron, η

$$\eta = <\varepsilon> + <S_n> \tag{16}$$

and the average prompt γ–ray energy[Tudora and Hambsch, 2017]:

$$<E_\gamma> = E^* - \nu\eta \tag{17}$$

<Sn> entering Eq.(16)is the averageneutron separation energy[Tudora and Hambsch, 2017] which takes into account the sequential neutron emission, as following:

$$<S_n>(A,Z) = \frac{1}{k}\sum_{i=0}^{k-1} S_n(A-i,Z) = \frac{S_{kn}(A,Z)}{k} \tag{18}$$

where k is the number of emissions sequences. The sequential emission stops when the excitation energy of the k-th nucleus becomes less than its neutron separation energy. According to Ref.[Tudora, et. al., 2015] the ratio $\nu_H(A)/\nu_{pair}(A)$ is well approximated by $E^*(A)/TXE(A)$[Tudora and Hambsch, 2017].

Consequently ν_L and ν_H of a given pair (fragmentation) can be obtained as: $\nu_H = r_H \nu_{pair}$, $\nu_L = r_L \nu_{pair}$, whereν_{pair} is obtained from the energy conservation [Tudora and Hambsch, 2017]:

$$TXE = \nu_{pair}\left(<\varepsilon> + <S_n>_{pair}\right) + <E_\gamma>_{pair} \Rightarrow \nu_p = \frac{TXE - <E_\gamma>_{pair}}{<\varepsilon> + <S_n>_{pair}} \tag{19}$$

where <ε> is the average prompt neutron energy in CMS (first order momentum of the Φ(ε) given by Eq. 11), $<S_n>_{pair}$ and $<E_\gamma>_{pair}$ are the average neutron separation energy and the average prompt γ-ray energy corresponding to a fragment pair[Tudora and Hambsch, 2017].

The energy deposition into the medium is defined by [Madland, 2006] for a fragment pair as:

$$E_{d(pair)} = Q + E_n + B_n - \nu_{pair} <S_n>_{pair} \tag{20}$$

Note, using the fragment kinetic energy (resulting from TKE by momentum conservation)i.e. $E_k^{L,H} / TKE = A^{L,H} / \left(A^L + A^H\right)$, the energy deposition in the medium can be expressed for a fragment as[Tudora and Hambsch, 2017]:

$$E_d = E_k + \nu < \varepsilon > + E_\gamma \quad (21)$$

All quantitiesmentioned above are calculated for a fragment or fragment pair at a given TKE value. As it was already mentioned any prompt emission quantity can be generically labeled q(A,Z,TKE)[Tudora and Hambsch, 2017].

II.4. Average Prompt Emission Quantities

Taking into account that the majority of experimental prompt emission data refer to single distributions or total average quantities, in order to compare the PbP model results with these data, the multi-parametric matrices q(A,Z,TKE) of different quantities are averaged over the fission fragment distribution Y(A,Z,TKE) in different ways as follows[Tudora and Hambsch, 2017]:

- quantities as a function of A (i.e. S_n(A), TXE(A), ν(A)):

$$\bar{q}(A) = \sum_{Z,TKE} q(A,Z,TKE) Y(A,Z,TKE) / \sum_{Z,TKE} Y(A,Z,TKE) \quad (22)$$

- quantities as function of TKE (i.e. ν(TKE), Eγ(TKE)):

$$< q > (TKE) = \sum_{A,Z} q(A,Z,TKE) Y(A,Z,TKE) / \sum_{A,Z} Y(A,Z,TKE) \quad (23)$$

- total average quantities (i.e. $<TXE>_{tot}$, $<\nu>_{tot}$):

$$< q >_{tot} = \sum_{A,Z,TKE} q(A,Z,TKE) Y(A,Z,TKE) / \sum_{A,Z,TKE} Y(A,Z,TKE) \quad (24)$$

In the PbP model any experimental or theoretical distribution Y(A,Z,TKE) can be employed[Tudora and Hambsch, 2017].

III. Results and discussions

III.1 Experimental fission fragment distributions used in the PbP model calculations for $^{235}U(n_{th},f)$

The multiple fission fragment distribution Y(A,Z,TKE) used in the PbP treatment is expressed as ([Capote et al., 2016] and references therein):

$$Y\left(A,Z,TKE\right)=Y_{\exp}\left(A,TKE\right)p(Z,A) \tag{25}$$

The double distribution Y_{exp}(A,TKE) entering Eq.(25) is re-constructed from the experimental single distributions Y(A), TKE(A) and σ_{TKE}(A) of $^{235}U(n_{th},f)$ available in the EXFOR library, according to the following expression [Capote et al., 2016]:

$$Y_{\exp}\left(A,TKE\right)=\frac{Y\left(A\right)}{\sigma\left(A\right)\sqrt{2\pi}}\exp\left(-\frac{\left(\mathrm{TKE}-\mathrm{TKE}\left(\mathrm{A}\right)\right)^{2}}{2\sigma_{\mathrm{TKE}}\left(\mathrm{A}\right)^{2}}\right) \tag{26}$$

These single distributions are the Y(A) and TKE(A) data of Nishio (plotted in **Fig.1** with blue squares) and of Surin [40112004,40112007] (red circles in Fig.1), and the TKE(A) and data of Asghar [21771014] (green diamonds in Fig.1). These experimental data allow to obtain two Y(A,TKE) distributions by using in Eq.(25) the data of Nishio and Surin and the σ_{TKE}(A) data of Asghar. As it can be seen in Fig.1, σ_{TKE}(A) data of Asghar exist only up to the mass fragmentation A_H=156, A_L=78. Accurate experimental Y(A,TKE) distributions were recently measured at JRC-Geel [Al-Adili,2013]for the fissioning system $^{234}U(n,f)$ at 14 incident neutron energies ranging from 0.2 to 5 MeV. The σ_{TKE}(A) data of $^{234}U(n,f)$ at En = 0.5 MeV shifted with one mass unit are plotted with wine circles in Fig.1. As it can be seen, they are very close to the data of Asghar and are available over a larger fragmentation range. Consequently these σ_{TKE}(A) data, together with the Y(A) and TKE(A) data of Nishio and Surin, are used in the re-construction of two Y_{exp}(A,TKE) distributions (which will be denoted in the following as Y(A,TKE) of Nishio and Surin).

The isobaric charge distribution p(Z,A) entering Eq.(25) is taken as a Gaussian function centered on the most probable charge Zp(A) (taken as the unchanged charge distribution Z_{UCD}(A) corrected with the charge polarization ΔZ(A)), i.e..

$$p\left(Z,A\right)=\frac{1}{rms\left(A\right)\sqrt{2\pi}}\exp\left(-\frac{\left(Z-Z_{p}\left(A\right)\right)^{2}}{2rms\left(A\right)^{2}}\right) \tag{27}$$

The charge polarization ΔZ(A) and the root-mean-square rms(A) of Wahl [Wahl, 1988], plotted in **Fig.2**, are used.

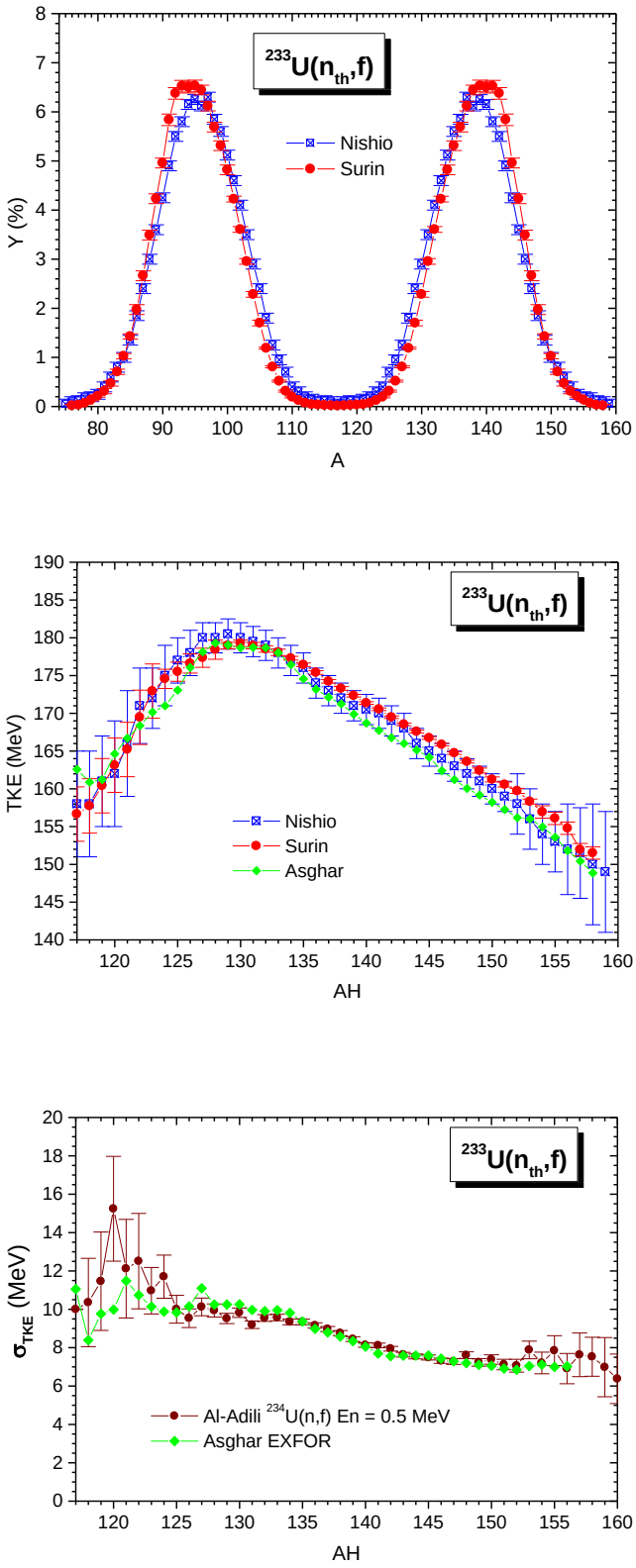

Fig.1: Experimental Y(A) (upper part), TKE(A) (middle) and σ_{TKE}(A) (lower part): the data of Surin (red circles), Nishio (blue squares with a cross inside), Asghar (green diamonds) and the data of Al-Adili et al. for ^{234}U(n,f) at E_n = 0.5 MeV shifted with one mass unit (wine squares).

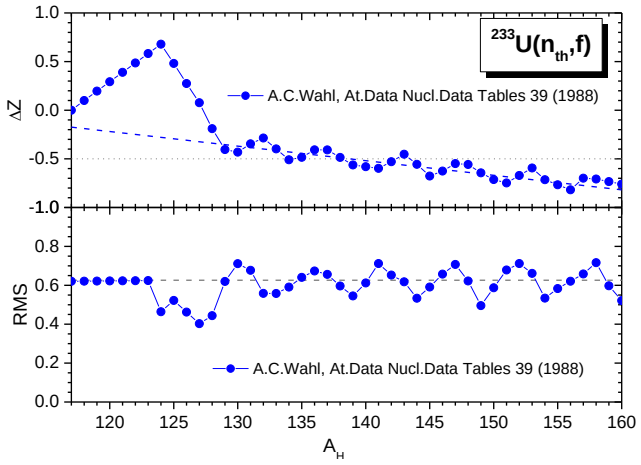

Fig.2: ΔZ(A) and rms(A) of Wahl for $^{233}U(n_{th},f)$.

III.2 Comparison of PbP model results for $^{233}U(n_{th},f)$ with the experimental data andthe results of a sequential emission treatment

As it was mentioned (e.g. Refs.[Tudora et al., 2018; Tudora and Hambsch, 2017; Capote et al. 2016] and references therein) the most reliable and significant validation of a prompt emission modeling consists in the comparison of the multi-parametric matrices of different quantities with the existing experimental data, because in this case the fission fragment distributions Y(A,TKE) are not involved.

Such prompt emission quantities, for which experimental data exist are the prompt neutron multiplicity ν(A,TKE) and the average prompt γ-ray energy Eγ(A,TKE). They were measured only for a few fissioning systems. As an example the ν(A,TKE) data for ^{252}Cf(SF) and ^{235}U(n,f) recently measured at JRC-Geel [Gook et al, 2014, 2017] and the Eγ(A,TKE) data of Nifenecker [Nifenecker,1973] described very well by the PbP model results (see Ref. [Tudora and Hambsch, 2017]) assured a detailed validation of the PbP calculations.

Fortunately, in the case of $^{233}U(n_{th},f)$ experimental ν(A,TKE) data measured by Nishio are available in the EXFOR library [22660008]. The multi-parametric matrix of prompt neutron multiplicity provided by the PbP model calculation is compared with these data by employing the following bi-dimensional representations:

- prompt neutron multiplicity as a function of TKE for a given light fragment mass (A_L) and heavy fragment mass (A_H) and to the fragment pair, in **Fig. 3.**
- prompt neutron multiplicity as a function of A for a given TKE value, in **Fig.4.**

In Fig.3 the experimental data of Nishio corresponding to 16 mass fragmentations (with A_L and A_H indicated in each frame) randomly chosen so that to cover almost the entire fragmentation range, are plotted with full gray circles (heavy fragment), open black squares (light fragment) and full black diamonds (fragment pair). The PbP model results are plotted with continuous lines, colored in blue for the heavy fragment, green for the light fragment and red for the fragment pair.

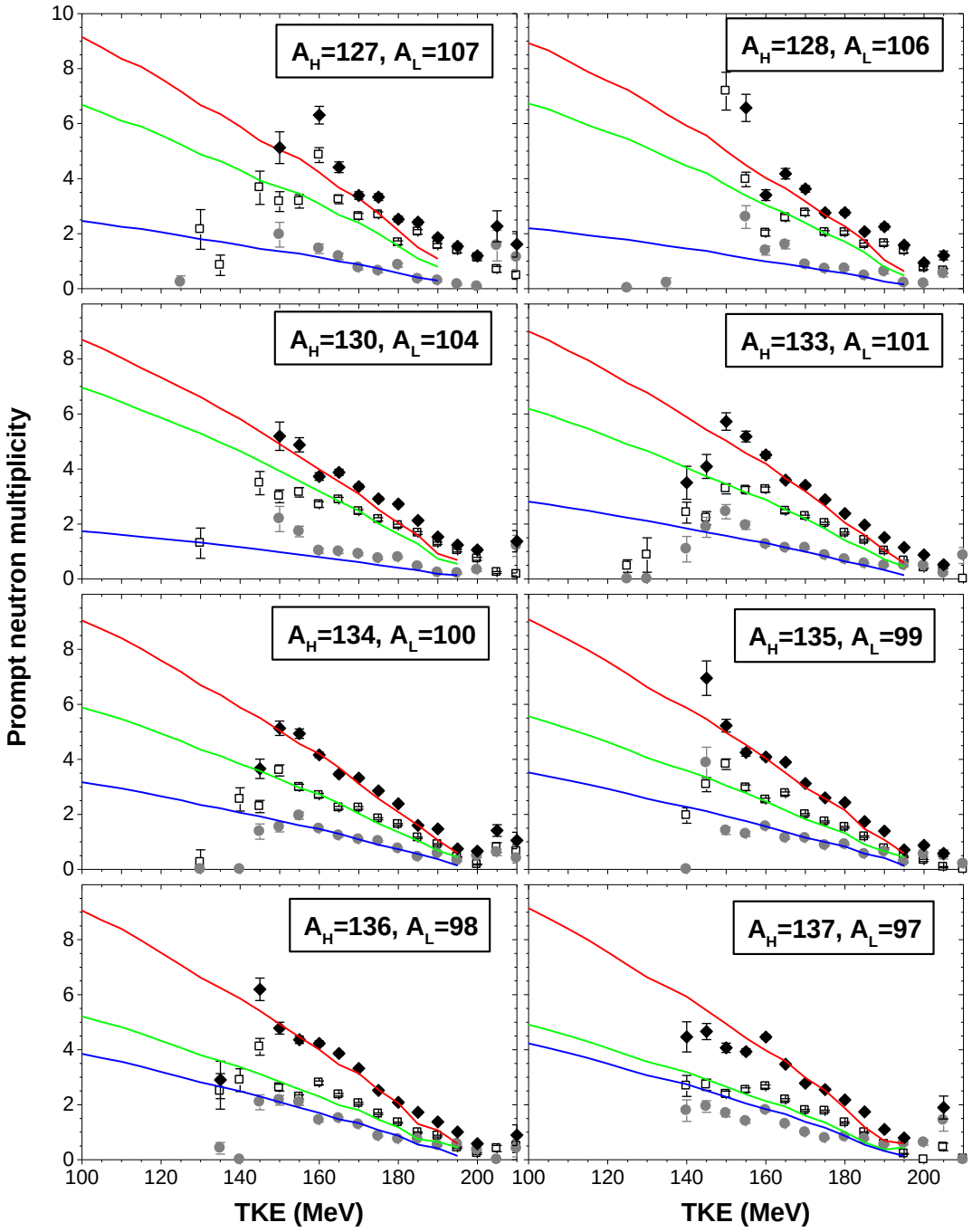

Fig.3a: ν(A,TKE) for $^{233}U(n_{th},f)$ plotted as a function of TKE for a given fragmentation (with A_L and A_H indicated in each frame): the data of Nishio (full gray circles for the heavy fragment, open black squares for the light one and full black diamonds for the pair) and the PbP results (a blue line for the heavy fragment, a green line for the light one and a red line for the fragment. pair).

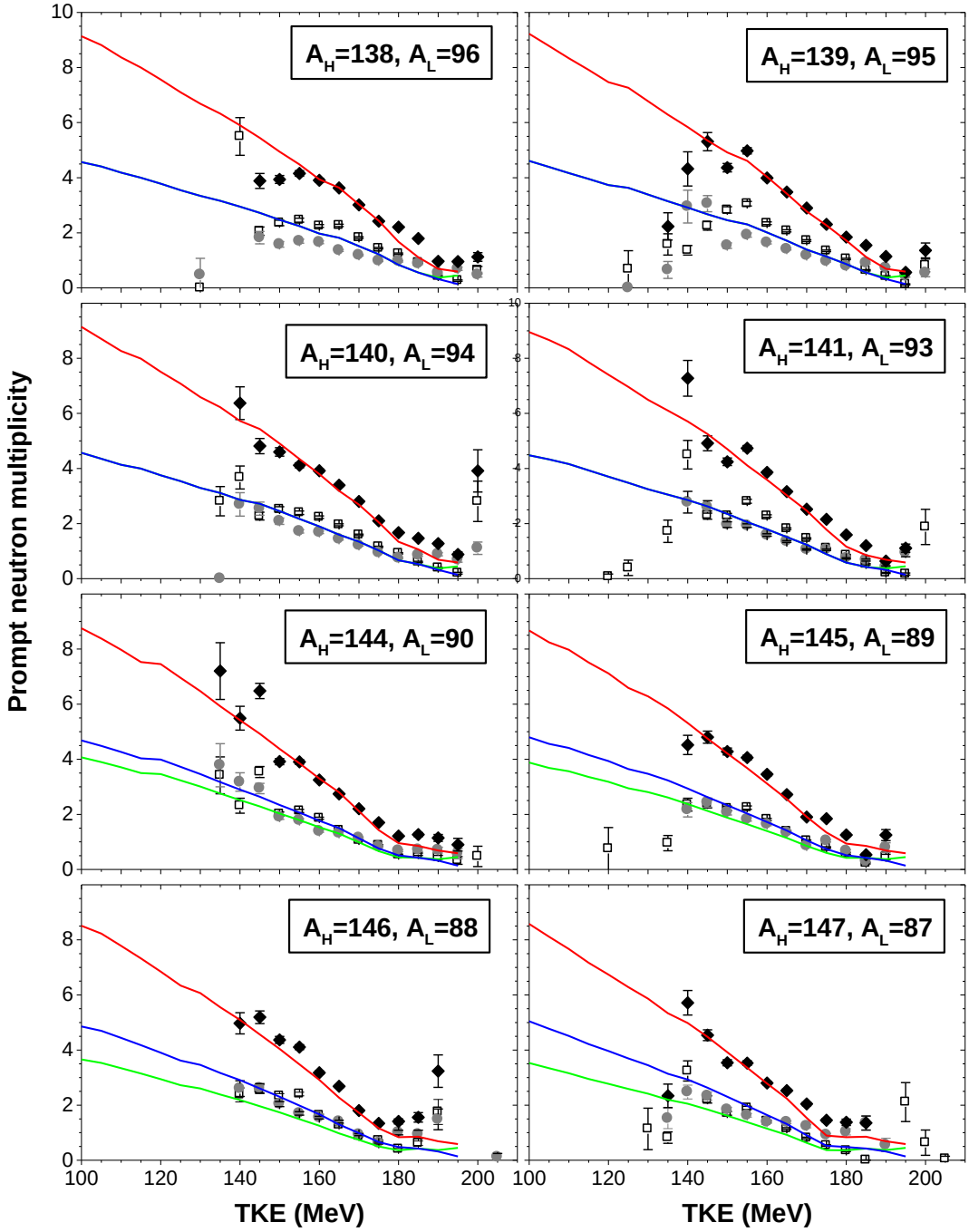

Fig.3b: ν(A,TKE) for $^{233}U(n_{th},f)$ plotted as a function of TKE for a given fragmentation (with A_L and A_H indicated in each frame): the data of Nishio (full gray circles for the heavy fragment, open black squares for the light one and full black diamonds for the pair) and the PbP results (a blue line for the heavy fragment, a green line for the light one and a red line for the fragment pair).

The good description of experimental ν(A,TKE) data by the PbP results is visible for all fragmentations.

Examples of prompt neutron multiplicity as a function of A for a given TKE value are plotted in **Fig.4** for eight TKE values indicated in each frame: the experimental data of Nishio with full black squares and the PbP results with full red circles.

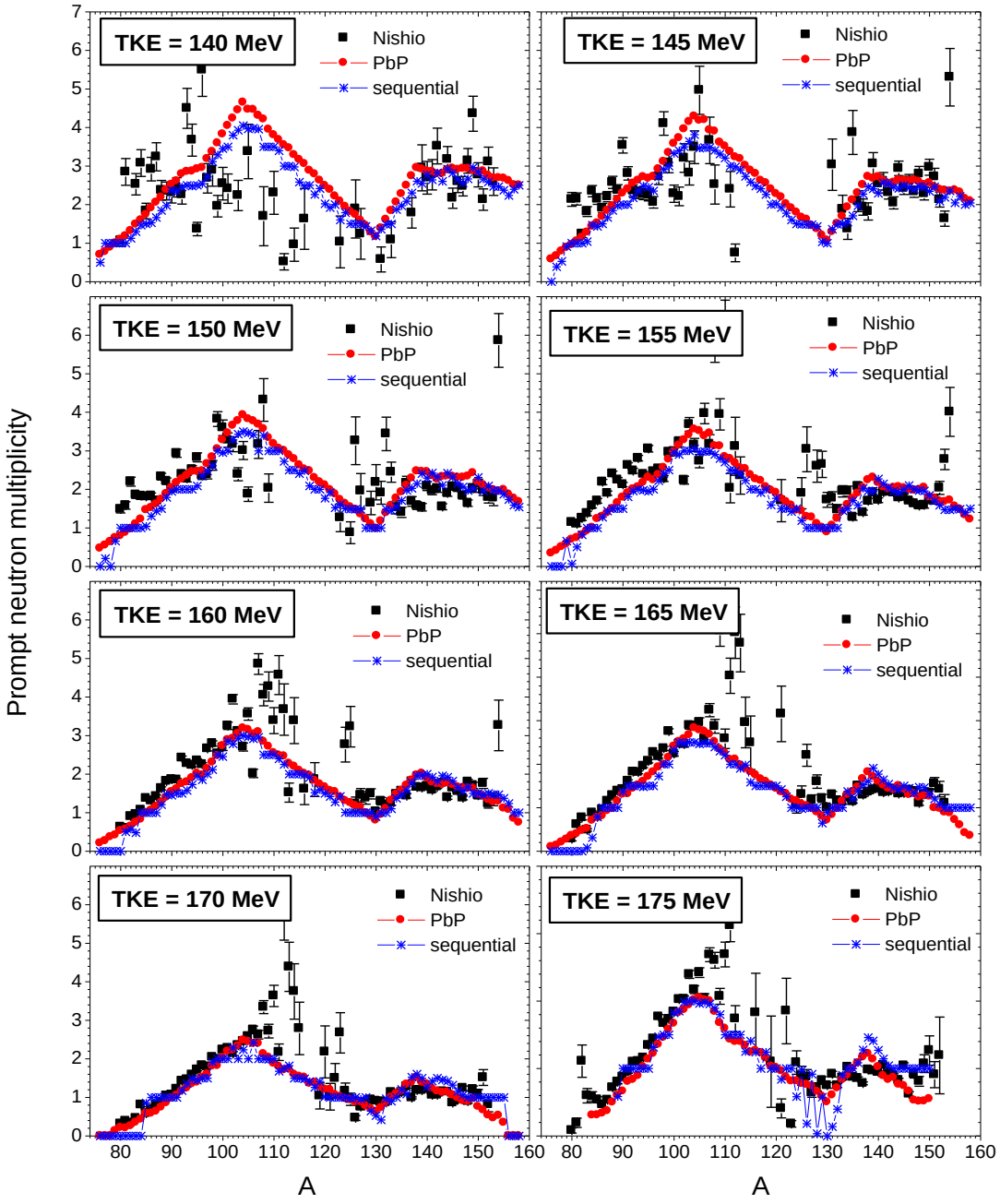

Fig.4: ν(A,TKE) for $^{233}U(n_{th},f)$ plotted as ν(A) for a given TKE value (indicated in each frame). The experimental data of Nishio are given with full black (squares, the PbP results with full red circles and the results of the sequential emission treatment with blue stars.

Both results, of the PbP and sequential emission modelings, are close to each other and describe well the experimental data of Nishio, which are spread especially at lower TKE

values (below ofabout 150 MeV). An underestimation of the spread experimental data at mass numbers nearsymmetry is visible at higher TKE values (above of about 160 MeV).

The ν(A,TKE) results of PbP can be also compared with the ν(A,TKE) results of the sequential emission treatment. To avoid very charged figures, ν(A,TKE) results provided by the sequential emission modeling (mentioned on item B2 in the introduction chapter) are given in **Appendix** (where they are plotted in the representation of prompt neutron multiplicity as a function of TKE for a given light and heavy fragment mass and the corresponding pair).

Different average prompt emission quantities as a function of A or as a function of TKE (e.g. ν(A), ν(TKE), Eγ(A), Eγ(TKE)) can be easily obtained by averaging the corresponding matrices, generically labeled as q(A,Z,TKE), over the Y(A,Z,TKE) distribution (by summing over Z and TKE and over A and Z, respectively). They are compared with the existing experimental data, too.

The PbP result of ν(A) (obtained by averaging ν(A,TKE) over the experimental Y(A,TKE) of Surin) is plotted in **Fig.5** with red circles together with the experimental ν(A) data taken from EXFOR: of Nishio [22660005] (full black squares), Fraser and Milton [14369004] (full gray diamonds) and Apalin [41397004](open black circles).

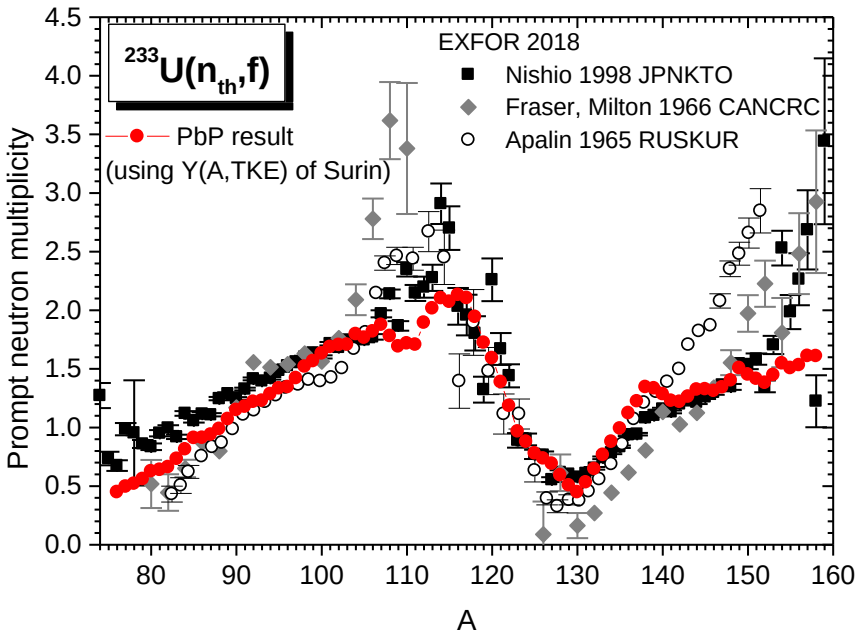

Fig.5: PbP result of ν(A) (full red circles) in comparison with the experimental data from EXFOR (different black and gray symbols).

As it can be seen the ν(A) of PbP describes well the data of Nishio over the entire mass range, except only the region of very asymmetric fission where a slow underestimation at AL less than 85 and a significant underestimation at A_H above 155 are observed. The PbP result also describes well the data of Fraser and Milton and of Apalin over the entire light fragment range. In the heavy fragment region it agrees with the data of Apalin up to A_H of

about 140 and with the data of Fraser and Milton up to A_H of about 130. Furthermore it is easily to seen that the ν(A) data of Fraser and Milton are too low at A_H around 130 and the data of Apalin exhibit a very pronounced increase at A_H above 140, deviating from the normal trend of the other data.

An unique experimental data set exists for ν(TKE) in the EXFOR library, i.e. of Nishio [2266007] which is plotted with full black squares in **Fig.6**.

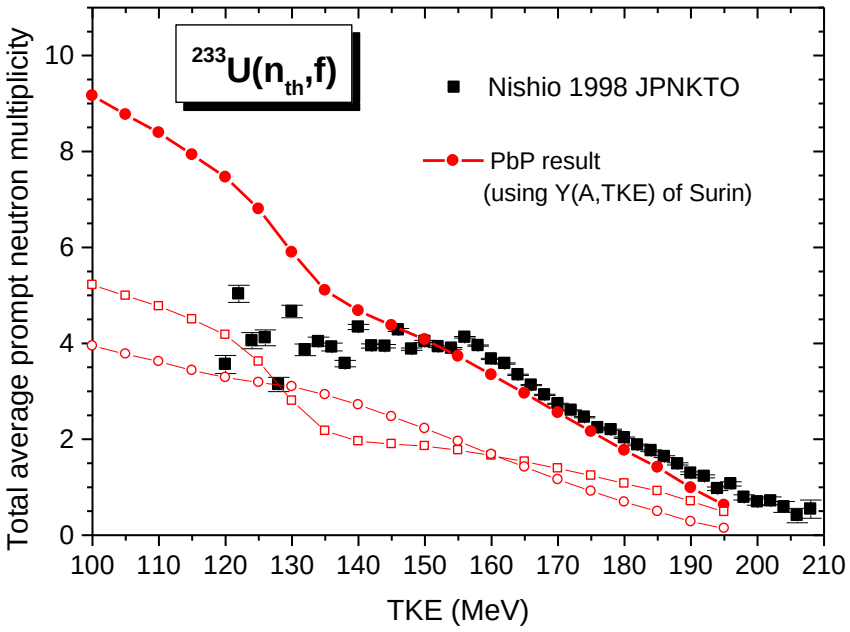

Fig.6: ν(TKE) of $^{233}U(n_{th},f)$: experimental data of Nishio (full black squares) and the PbP result (red symbols).

The ν(TKE) result of PbP (obtained by averaging ν(A,TKE) over the experimental Y(A,TKE) of Surin), plotted with full red circles connected with a solid line is in a reasonable agreement with these data at medium and high TKE values, where the decreasing slope of the PbP result and the experimental data is the same and only a very slow underestimation of the data is observed. At low TKE values (below of 150 MeV) the data of Nishio are spread and they exhibit an unphysical behaviour, which is due to the experimental treatment, as it was demonstrated in Ref.[Gook and al., 2014]. The PbP results of ν_L(TKE) (open red squares) and ν_H(TKE) (open red circles) are also given in Fig.6.

Experimental prompt γ-ray data for $^{233}U(n_{th},f)$ exists, too. They were measured by Pleasonton [Pleasonton, 1973] and refer to the average prompt γ-ray energy as a function of A, Eγ(A), and average prompt γ-ray multiplicity as a function of A, Nγ(A). The Eγ(A) and Nγ(A) data of Pleasonton are plotted with full black squares in **Fig. 7** (upper and lower part, respectively). As it can be seen, the PbP results of Eγ(A) and Nγ(A) (obtained by averaging the matrices Eγ(A,TKE) and Nγ(A,TKE) over the experimental Y(A,TKE) of Surin), given with full red circles, are in very good agreement with the data of Pleasonton.

It is well known that a linear correlation exists between the prompt γ-ray energy and the prompt neutron multiplicity. This correlation was firstly experimentally observed by Nifenecker (in the case of ^{252}Cf(SF)) and Fréhaut [Fréhaut, 1989)] (for the neutron induced fission of ^{232}Th, ^{235}U, ^{237}Np). For each investigated fissioning nucleus, they have reported slope and intercept values of the linear correlation.

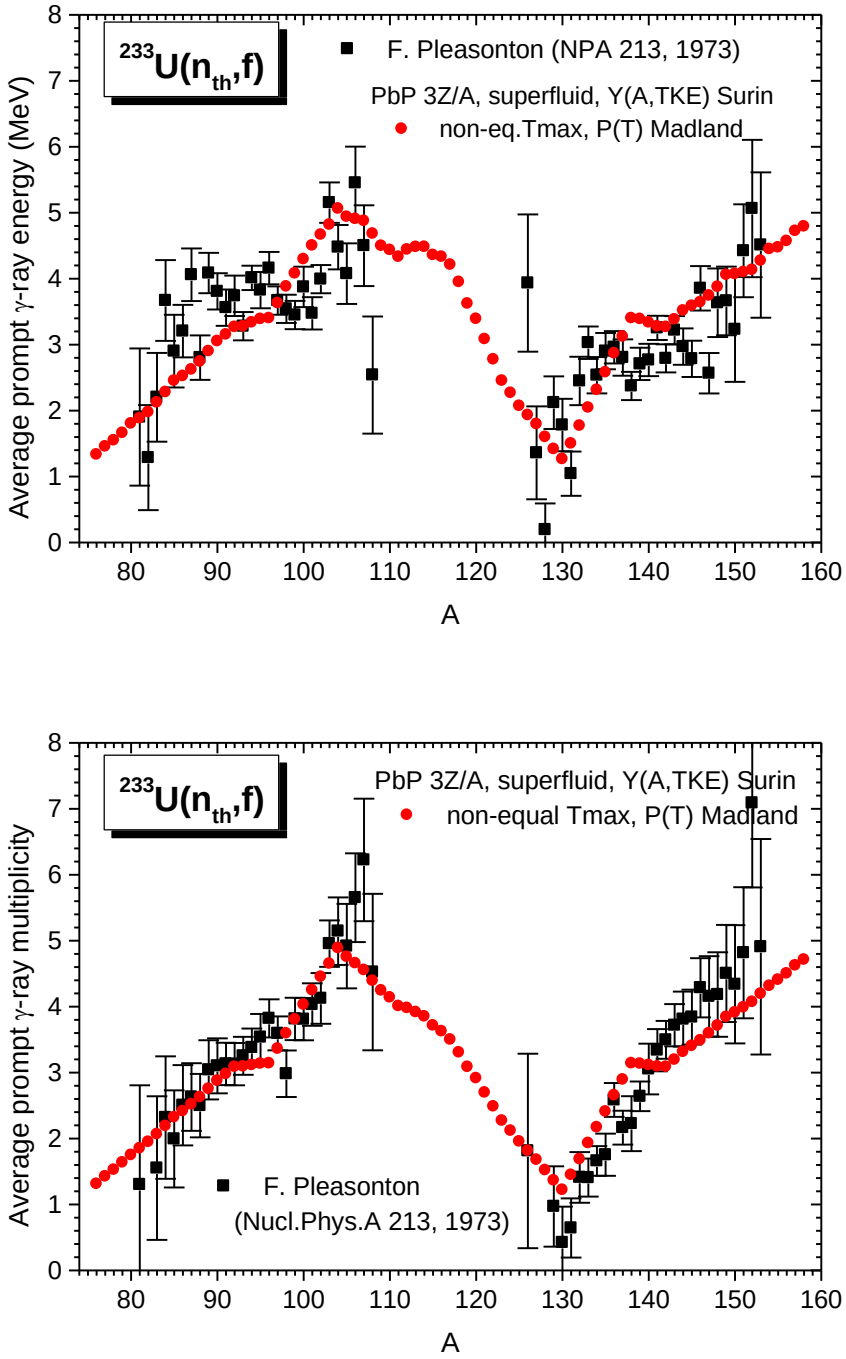

Fig.7: PbP model results (red circles) of average prompt γ-ray energy (upper part) and average prompt γ-ray multiplicity (lower part) as a function of A in comparison with the experimental data of Pleasonton (black squares).

A general systematic for the slope p and the intercept q of the linear correlation $< E_\gamma >= p < \nu > + q$ (which are expressed only as a function of the charge and mass numbers of the fissioning nucleus) was developed by Vladuca and Tudora [Vladuca and Tudora, 2001a,b,c] and [Tudora, 2009]: $p = 6.71 - 0.156\, Z_0^2 / A_0$, $q = 0.75 + 0.088\, Z_0^2 / A_0$ (where Z_0 and A_0 refer to the fissioning nucleus).

The linear correlation resulting from the present PbP results of ν(TKE) and Eγ(TKE) is plotted with red circles in **Fig.8**. Its linear fit is plotted with a red line. The linear dependence given by the systematic of Vladuca and Tudora for the case of ^{234}U is plotted with a black dashed line. The good agreement of the correlation resulting from the present PbP calculations with the correlation based on the p and q systematic is visible.

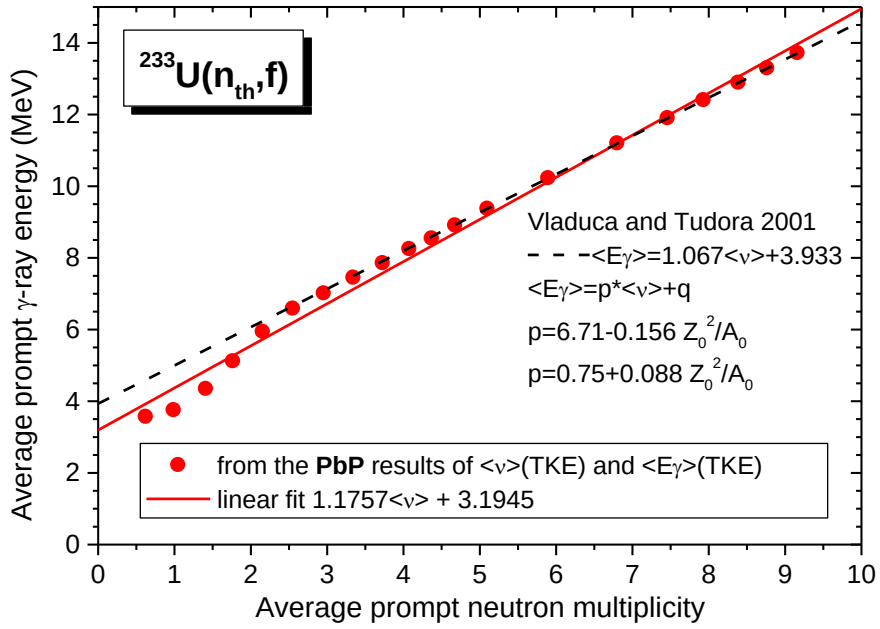

Fig.8: The linear correlation between the prompt γ-ray energy and the prompt neutron multiplicity resulting from the PbP results of <ν>(TKE) and <Eγ>(TKE) (red circles). Its linear fit is plotted with a red line. The linear correlation expressed by the general parameterization of Vladuca and Tudora is plotted with a dashed black line.

Beside the probabilistic treatment of the sequential emission included in the Monte-Carlo codes FIFRELIN, CGMF, FREYA and GEF (mentioned at the beginning of Chapter II) a determinist treatment of the sequential emission was recently developed as the University of Bucharest [Tudora et al., 2018]and [Tudora and Hambsch, 2018]. This treatment, based on recursive equations of the residual temperatures, was applied to numerous cases of spontaneous fission and neutron-induced fission. This allowed to determine a new triangular form of the residual temperature distribution P(T) entering the prompt emission models with a global treatment of the sequential emission. More details about this new sequential emission modeling and P(T) can be found in Ref.[Tudora et al., 2018].

Another validation of the present PbP results for $^{233}U(n_{th},f)$ is the comparison with the results of this new modeling of sequential emission in which the same fragmentation range as in the PbP treatment was considered. The prescriptions concerning compound nucleus cross-sections of the inverse process of neutron evaporation from fragments $\sigma_c(\varepsilon)$ and the level density parameters of fragments differ from the ones used in the PbP calculation. I.e. an analytical expression of $\sigma_c(\varepsilon)$ based on the average s-wave neutron strength function (parameterized as a function of the mass number of initial and residual fragments) and non-energy dependent level density parameters provided by the Egidy-Bucurescu systematic for the back-shift Fermi-gas model were employed (details are given in Ref. [Tudora et al., 2018] and references therein). The same experimental Y(A,TKE) distribution (of Surin) is used in the sequential emission calculation, too.

In **Figs. 9-11** the PbP results of ν(A), ν(TKE) and Eγ(A) are compared with the results of the sequential emission modeling. The PbP results are plotted with full red circles and the ones of the sequential emission treatment with blue stars. The experimental data are also given with the same symbols and colors as in the previous figures.

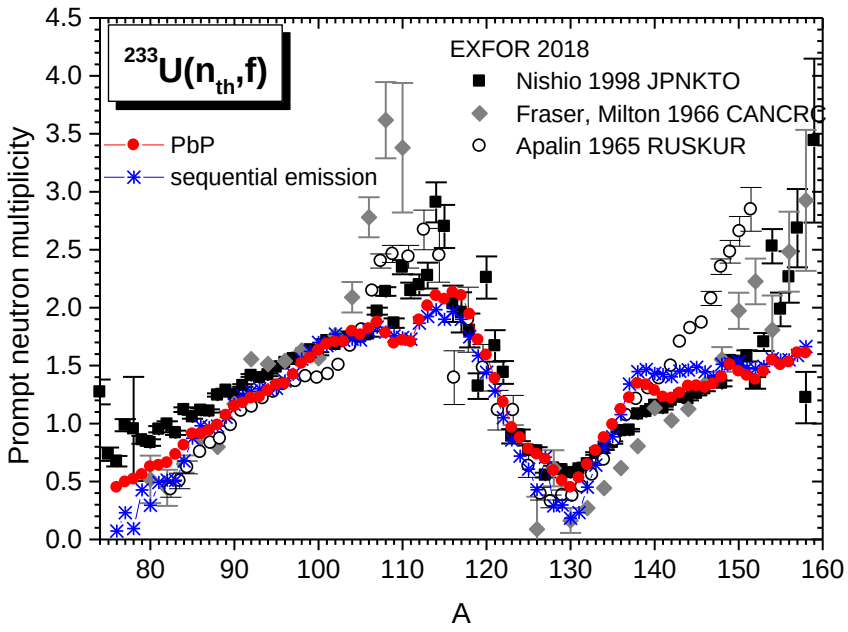

Fig.9: PbP result of ν(A) of $^{233}U(n_{th},f)$ (full red circles) in comparison with the result of the sequential emission modeling of Ref.[Tudora et al., 2018] (blue stars) and the experimental data taken from EXFOR (different black and gray symbols).

As it can be seen in **Fig.9**, ν(A) of PbP is close to the sequential emission result over the entire A range, except for A below 85 where ν(A) of sequential emission calculation is lower and describes very well the experimental data of Apalin (open black circles) and of Fraser and Milton (full gray diamonds). At A around 130, the sequential emission result is lower than the PbP result being in agreement with the data of Fraser and Milton. At A between 138 and 145 the sequential emission result slightly overestimates the experimental data and the PbP result.

The same good agreement between the PbP and sequential emission calculations is seen in the case of the ν(A,TKE) matrices represented in Fig.4 as ν(A) for a given fragmentation.

As it can be seen in **Fig.10,** the ν(TKE) results of PbP and sequential emission are very close to each other at TKE value above 155 MeV and they exhibit the same decreasing slope At lower TKE values (below of about 150 MeV) the sequential emission result is lower than the PbP result. The same trend is observed in the case of the components ν_L(TKE) and ν_H(TKE).

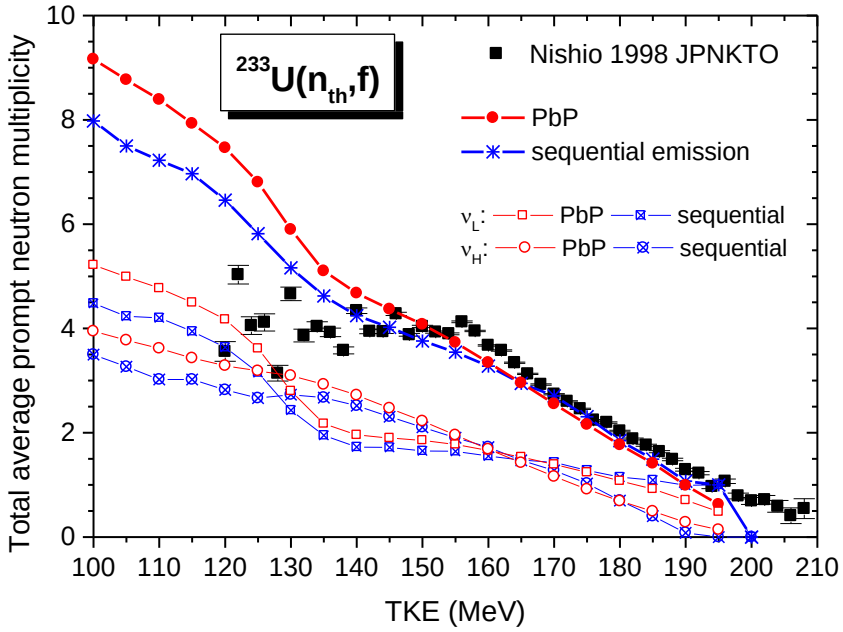

Fig.10: PbP results of ν(TKE) (full red circles), ν_L(TKE) (open red squares) and ν_H(TKE) (open red circles) in comparison with the sequential emission results of ν(TKE) (blue stars), ν_L(TKE) (blue squares with a cross inside) and ν_H(TKE) (blue circles with a cross inside) and the experimental data of Nishio (full black squares).

This behavior at lower TKE values is not surprising because the successive neutron emission from only three initial fragments at each A and TKE is taken into account. While in the PbP calculation, While the triangular residual temperature distribution P(T) (over which the evaporation spectrum is integrated) which is used in the PbP model assures a global and complete consideration of the sequential emission (i.e. more emitted neutrons than from the 3 fragments taken at each A and TKE).

This fact also explains the staggering observed in the ν(A,TKE) results of the sequential emission modeling given in **Appendix**, where they are plotted as a function of TKE for each A in the. It can be observed that for a great part of mass pairs (e.g. {137,97}, {138,96}, {139,95}, {140,94}, {141,93}, {142,92}, {143,91}, {144,90}, …{147,87} the staggering of the result plotted with a wine line (the prompt neutron multiplicity of the pair) reproduces perfectly the experimental data plotted with full black diamonds.

The sequential emission result of Eγ(A), plotted in **Fig.11** with blue stars, exhibits a staggering behaviour which seems to give a better description of the experimental data of Pleasonton (full black squares) which also shows a staggering, compared to the smooth behaviour of the PbP result (red circles).

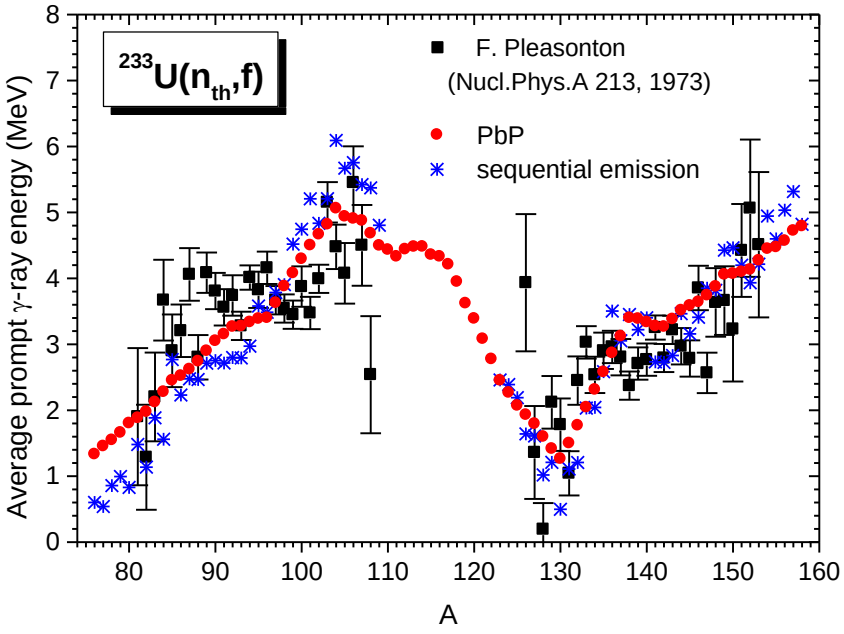

Fig.11: Eγ(A) of $^{233}U(n_{th},f)$ provided by the PbP (full red circles) and sequential emission (blue stars) calculations in comparison with the data of Pleasonton (full black squares).

III.3 Other results of the PbP model calculation

Total average quantities (obtained by averaging the corresponding multi-parametric matrices q(A,Z,TKE) over Y(A,Z,TKE) by summing over A, Z and TKE) characterizing both the fission fragments and the prompt emission are useful, too. The total average values of different quantities characterizing the fragments (e.g. excitation energies and level density parameters at full acceleration, average neutron separation energies from fragments) can be used as input in the well-known Los Alamos model working with only one fragmentation (the so-called "most probable fragmentation approach"). The total average values of different prompt emission quantities are required in multiple applications of fission, especially nuclear reactors, e.g. the total average prompt neutron multiplicity is a nuclear data required in the evaluated nuclear data libraries (MF=1, MT=456) being one of the four factors entering K_∞, the prompt neutron spectrum is the weighting function of the fast neutron group in the multi-group treatment of nuclear reactors, the total average prompt γ-ray energy is also required in the nuclear reactor design etc.

Examples of other quantities provided by the PbP model are given in the next figures, as follows.

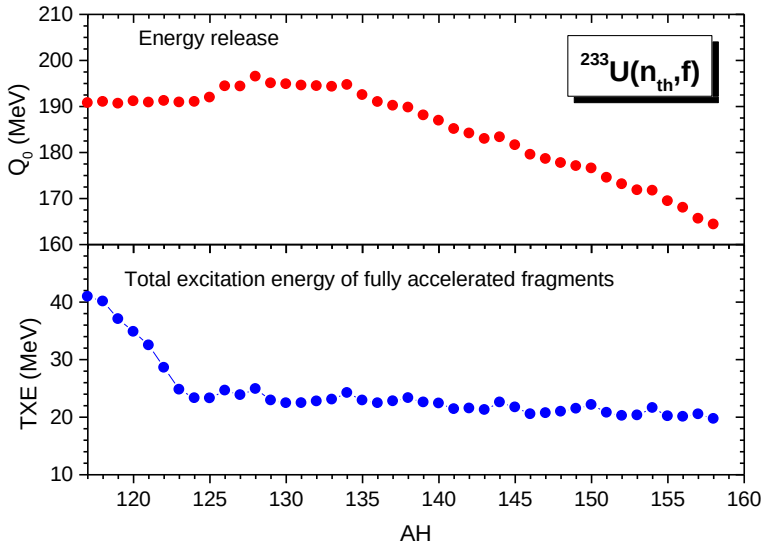

Fig.12: Average energy release (upper part) and TXE (lower part) as a function of A_H resulting from corresponding the multi-parametric matrices of the PbP treatment averaged over the Y(A,Z,TKE) distribution by summing over Z and TKE.

Fig.**12** shows the average energy release in fission and the average total excitation energy at full acceleration as a function of the heavy fragment mass. The fragment excitation energy at full acceleration E*(A) resulting from the TXE partition based on modeling at scission (described in Refs. [Tudora and Hambsch, 2017] and [Tudora et al., 2015] and references therein) is plotted in **Fig.13**.

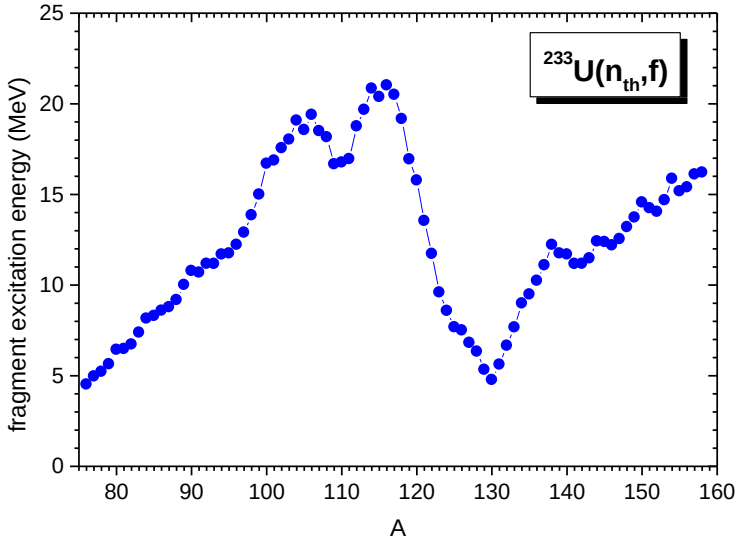

Fig.13: E*(A) of ^{233}U(n$_{th}$,f) resulting from the TXE partition based on modeling at scission, which is used in the PbP model.

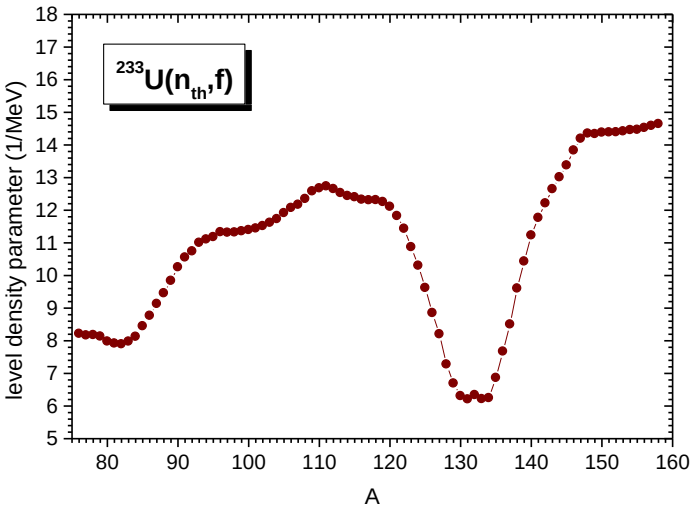

Fig.14: Level density parameter of fully accelerated fragments of ^{233}U(n$_{th}$,f) (provided by the super-fluid model) as a function of A.

The average level density parameters of fully accelerated fragments are plotted as a function of A in **Fig.14**. They are provided by the super-fluid model, in which the shell corrections of Moller and Nix and the parameterizations of Ignatiuk for the dumping of shell effects γ and the asymptotic level density parameter $\tilde{a}$ were used.

The average neutron separation energy from fully-accelerated fragments, obtained according to eq. (18), by taking into account the sequential emission Sn(A,Z,TKE) is averaged over the Y(A,Z,TKE) distribution (by summing over Z and TKE), giving <Sn>(A) which is plotted in **Fig.15**.

The low values of average S_n at A around 130 is due to the presence of magic and double magic heavy fragments (with N=82 and/or Z=50) with higher neutron separation energies than the neighboring nuclei concomitantly with the low values of their excitation energy, see Fig. 13 where the low E*(A) at A_H around 130 are visible. Consequently a great part of these heavy fragments cannot emit prompt neutrons (their excitation energy being lower than the neutron separation energy) leading to low values of the average S_n (obtained by averaging the matrix of neutron separation energy over the fragment distribution). The same situation is happening in the case of light fragments with A_L below 80 for which in many cases the excitation energy $E^*(A)$ being low (less than the neutron separation energy from the respective fragment) the prompt neutron emission cannot take place.

PbP results of other prompt emission quantities of ^{233}U(n$_{th}$,f) for which the experimental data are missing are given as following.

The average prompt neutron energy in the center-of-mass frame as a function of A and as a function of TKE is plotted in **Fig.16**.

The energy carried away per neutron is defined for each fragment {A,Z} at each TKE as $\eta = < \varepsilon > + < S_n >$ (where <ε> is the average prompt neutron energy in the center-of-mass frame and <Sn> the average neutron separation energy). The average energy carried away per neutron as a function of A and as a function of TKE (obtained by averaging the matrix

η(A,Z,TKE) over Y(A,Z,TKE) by summing over Z and TKE and over A and Z, respectively) is plotted in **Fig.17**.

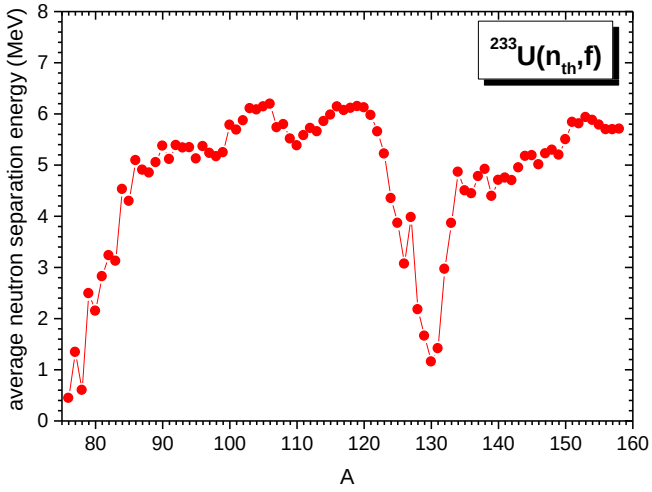

Fig.15: Average neutron separation energy from fully-accelerated fragments of ^{233}U(n$_{th}$,f) as a function of A.

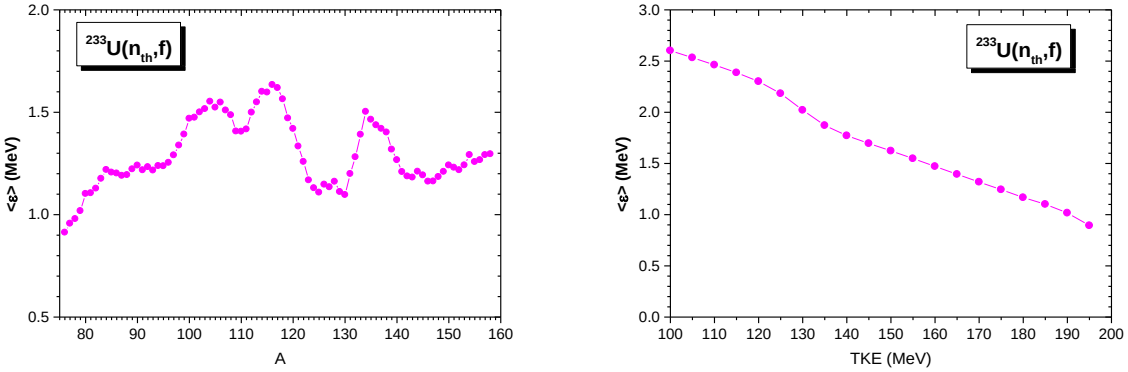

Fig.16: PbP results of the average prompt neutron energy in the center-of-mass frame for ^{233}U(n$_{th}$,f) plotted as a function of A (left part) and as a function of TKE (right part).

The prompt fission energy deposition in the medium was firstly defined by Madland [Madland, 2006] for a fragment pair at a given TKE, see eq. (20). The PbP result of the average energy deposition as a function of heavy fragment mass is plotted in **Fig.18a**

Taking into account the energy conservation for each fragmentation, the prompt fission energy deposition in the medium corresponding to an individual fragment at a given TKE can be also obtained according to Ref. [Tudora and Hambsch, 2017], see eq. (17). The average energy deposition as a function of A (obtained by averaging the PbP matrix E_d(A,Z,TKE) over Y(A,Z,TKE) by summing over Z and TKE) is plotted in **Fig.18b**.

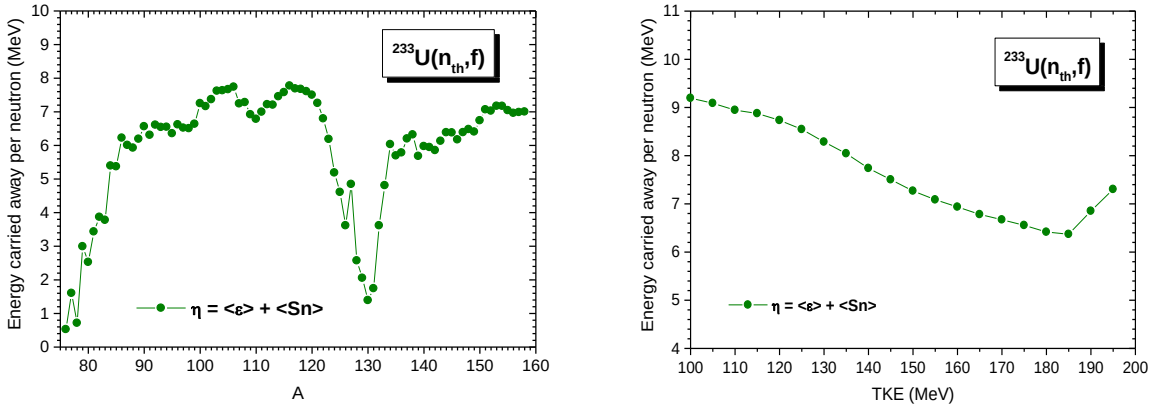

Fig.17: PbP results of the average energy carried out per neutron for ^{233}U(n$_{th}$,f) plotted as a function of A (left part) and as a function of TKE (right part).

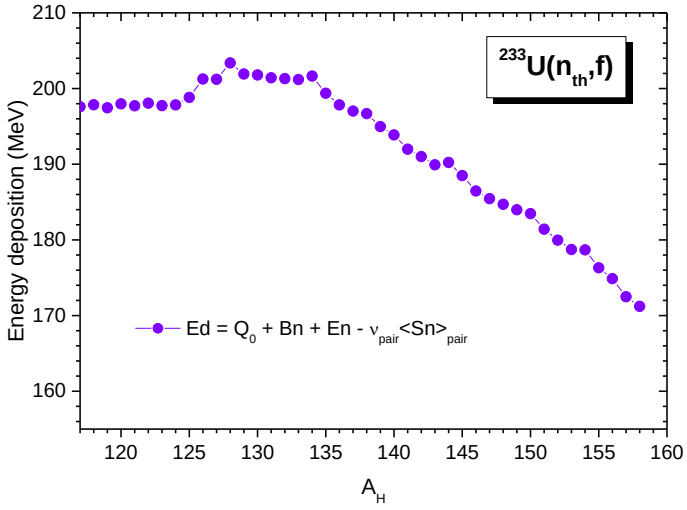

a)

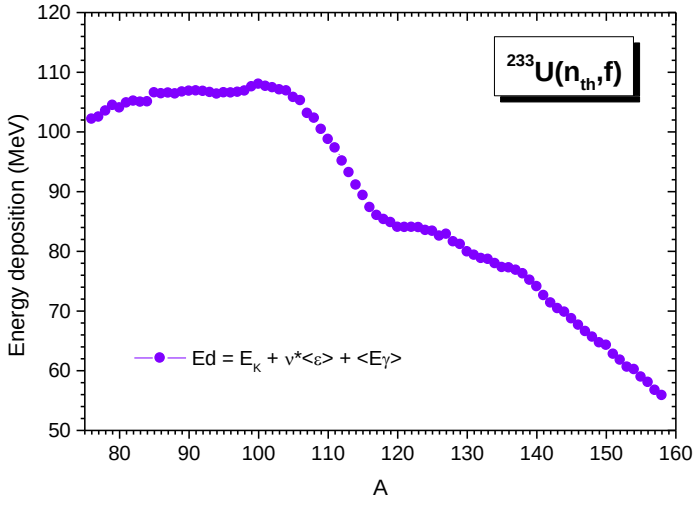

b)

Fig.18: The PbP result of Ed for: a).^{233}U(n$_{th}$,f) calculated according to the definition of Madland [Madland, 2006] plotted as a function of A$_H$ and b). ^{233}U(n$_{th}$,f) calculated according to the definition from Ref.[Tudora and Hambsch, 2017] plotted as a function of A.

Total average values of different quantities obtained in the frame of the PbP model are summarized in **Table 1**. In the averaging the Y_{exp}(A,TKE) distribution of Surin was used.

Table 1. Total average quantities resulting from the PbP treatment

Quantity	Value	Comments
$<Q_0>$ (MeV)	187.55	
<TKE> (MeV)	171.90	In agreement with the experimental data given in EXFOR
<TXE> (MeV)	22.495	
$<E^*_L>$, $<E^*_H>$ (MeV)	12.303 10.193	from the TXE partition based on modeling at scission
$<a_L>$, $<a_H>$ (MeV-1)	10.878 10.110 11.374 11.267	Super-fluid model, δW Moller and Nix, param. Ignatiuk Egidy-Bucurescu systematic for the BSFG model
$<C> = A_0/<a>$ (MeV)	11.15	Very close to the value of 11 MeV currently used in the LA model.
$<Sn_L>$, $<Sn_H>$ (MeV)	5.5181 5.1642	
<ν>	2.4811	In very good agreement with the experimental data from EXFOR and the values given in the last released versions of evaluated nuclear data libraries.
<Eγ> (MeV)	6.5811	In good agreement with the experimental data of Pleasonton <Eγ> = (6.69 ± 0.30) MeV
<Nγ>	6.197	In good agreement with the experimental data of Pleasonton <Nγ> = (6.31 ± 0.30) MeV

A comparison of prompt emission results obtained in this work with those provided by the GEF code is given in Appendix.

IV. Conclusions

Model calculation results of almost all quantities characterizing both the fission fragments and the prompt emission of the fissioning system $^{233}U(n_{th},f)$ are for the first time reported.

The deterministic prompt emission model Point-by-Point, developed at the University of Bucharest, was used to calculate these prompt emission quantities.

The computer code including the PbP model, written by the author of this model in FORTRAN95, was re-written in the Python interpreter language in the frame of this work.

Because the calculated multi-parametric matrices of different prompt emission quantities do not depend on the fission fragment distributions, the comparison of these matrices with existing experimental data constitutes the most relevant validation of a prompt emission modeling. Fortunately in the case of $^{233}U(n_{th},f)$ experimental data of the double distribution of prompt neutron multiplicity (A,TKE) exist. The very good description of these data by the PbP model result of ν(A,TKE) constitutes the most important validation of the present calculation.

The existence of other experimental prompt emission data for $^{233}U(n_{th},f)$, i.e. the single distributions of the prompt neutron multiplicity ν(A) and ν(TKE), the prompt γ-ray energy Eγ(A), and the prompt γ-ray multiplicity Nγ(A), which are very well described by the present PbP model results, assures a reliable supplementary validation of the PbP model together with the experimental Y(A,TKE) data (which have served to obtain the prompt emission single distributions mentioned above by averaging the corresponding multi-parametric matrices over these fragments distributions).

The linear correlation between the prompt γ-ray energy and the prompt neutron multiplicity resulting from the present PbP model calculation is in very good agreement with the systematic of this correlation (giving the slope and the intercept of the linear correlation only as a function of the charge and mass numbers of the fissioning nucleus).

The results reported in this dissertation are also in very good agreement with the results of a sequential emission modeling recently developed at the University of Bucharest, this comparison being a supplementary validation of the present PbP model results for $^{233}U(n_{th},f)$.

PbP model results of other quantities characterizing the fragments and the prompt emission for which experimental data do not exist are also reported, e.g. average prompt neutron energy in the center-of-mass frame $<\varepsilon>$(A) and $<\varepsilon>$(TKE), energy release Q(A), total excitation energy of fully accelerated fragments TXE(A), fragment excitation energy at full acceleration E*(A), level density parameter of fully-accelerated fragments a(A), energy carried away per neutron η(A) and η(TKE), prompt fission energy deposition in the medium Ed(A). Taking into account that these results are obtained concomitantly (in the same run) with the ones describing very well the existing experimental data, they can be considered as reliable predictions.

Total average values of important quantities are also reported. The obtained total average values of the energy release, the level density parameter and the neutron separation

energy can be used as input for the most probable fragmentation approach (Los Alamos model). The reported total average values of the prompt neutron multiplicity and the prompt γ-ray energy and multiplicity are in very good agreement with the experimental data, too.

Appendix

The prompt neutron multiplicity matrix ν(A,TKE) resulting from the sequential emission treatment of Ref. [Tudora et al., 2018]) applied to the fissioning system ^{233}U(n$_{th}$,f) is illustrated in Figs.A1 andA2 in comparison with the ν(A,TKE) data of Nishio (plotted with the same symbols and colors as in Fig.3a,b. The sequential emission results are plotted with continuous lines colored in dark yellow (light fragment), violet (heavy fragment) and wine (fragment pair).

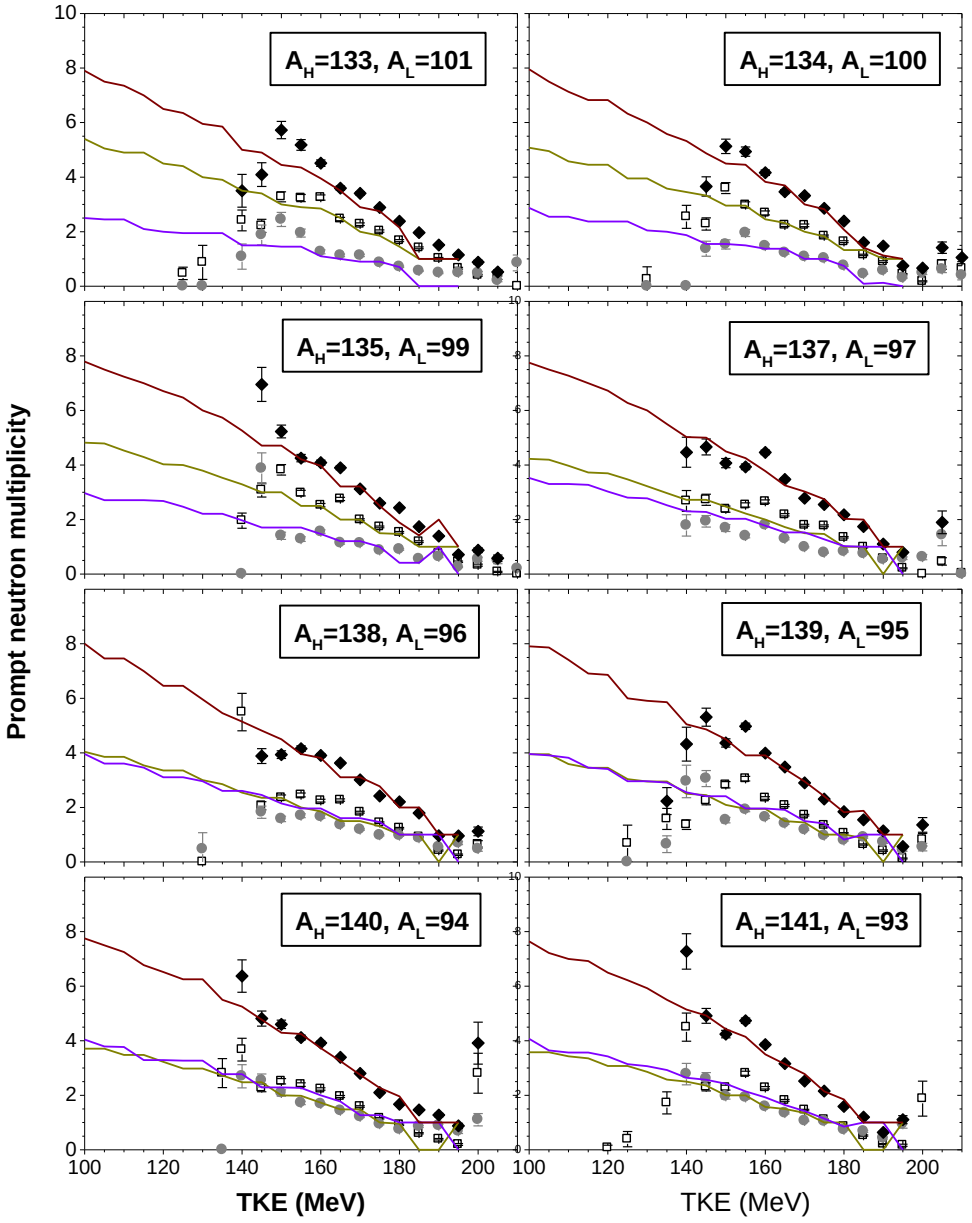

Fig.A1: Examples of ν(A,TKE) of ^{233}U(n$_{th}$,f) resulting from the sequential emission plotted as a function of TKE for a given fragmentation (with A_L and A_H indicated in each frame) with solid lines colored in violet (heavy fragment), dark yellow (light fragment) and wine (fragment pair) in comparison with the data of Nishio plotted with the same symbols and colors as in Fig.3a,b.

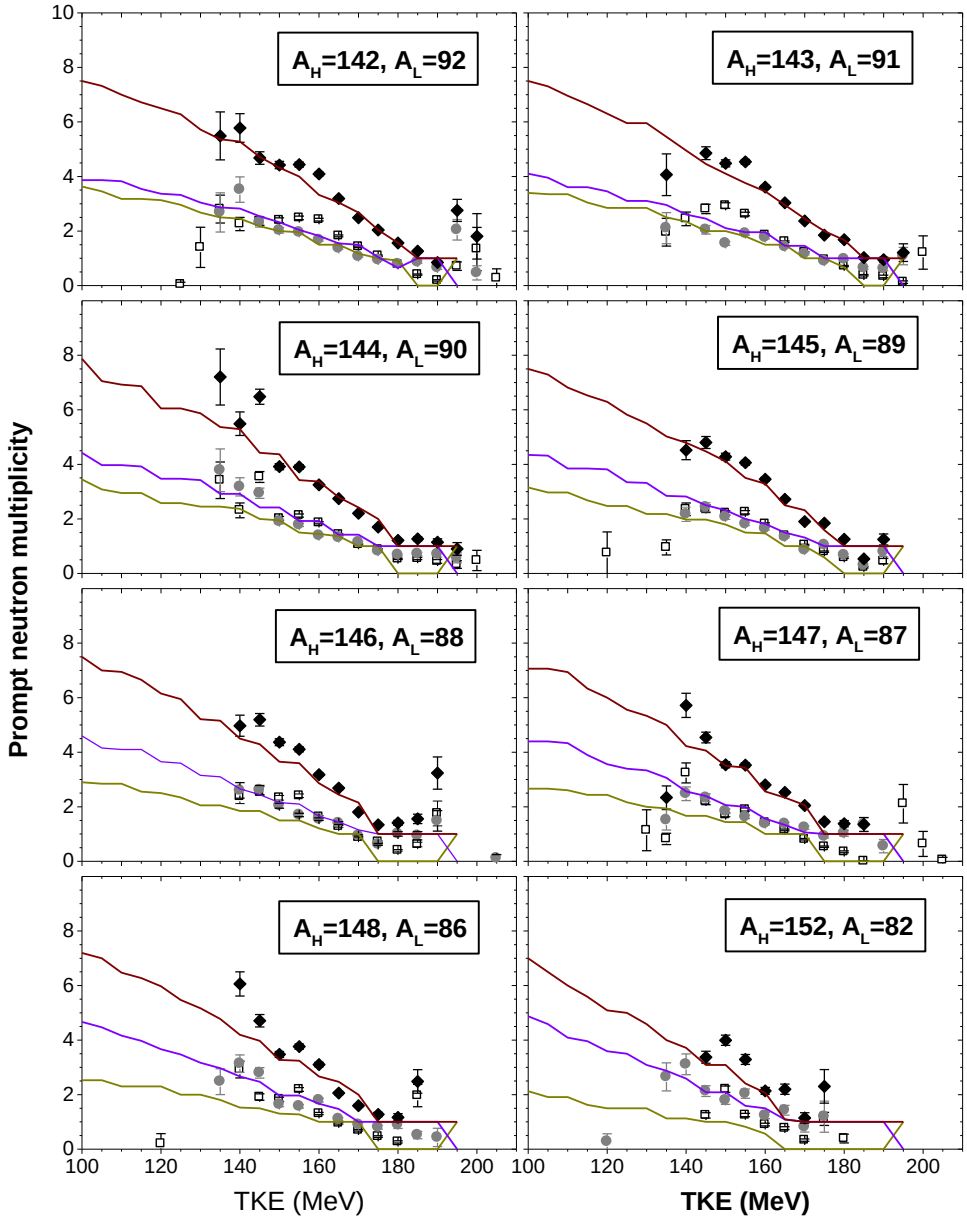

Fig.A2: Examples of ν(A,TKE) of $^{233}U(n_{th},f)$ resulting from the sequential emission plotted as a function of TKE for a given fragmentation (with A_L and A_H indicated in each frame) with solid lines colored in violet (heavy fragment), dark yellow (light fragment) and wine (fragment pair) in comparison with the data of Nishio plotted with the same symbols and colors as in Fig.3a,b.

Comparison of present results with those of the GEF code

The prompt emission results of the PbP model obtained in this work are compared with the results of the semi-empirical prompt emission code GEF [Schmidt and al., 2016]. The GEF results used in this comparison are provided by the version of 2015 (with default options and 10^5 events). The comparison of ν(A) and ν(TKE) provided by the PbP (red

circles) and sequential emission (blue synbols) modelings with the results of GEF (green symbols) is given in **Fig.A3.**

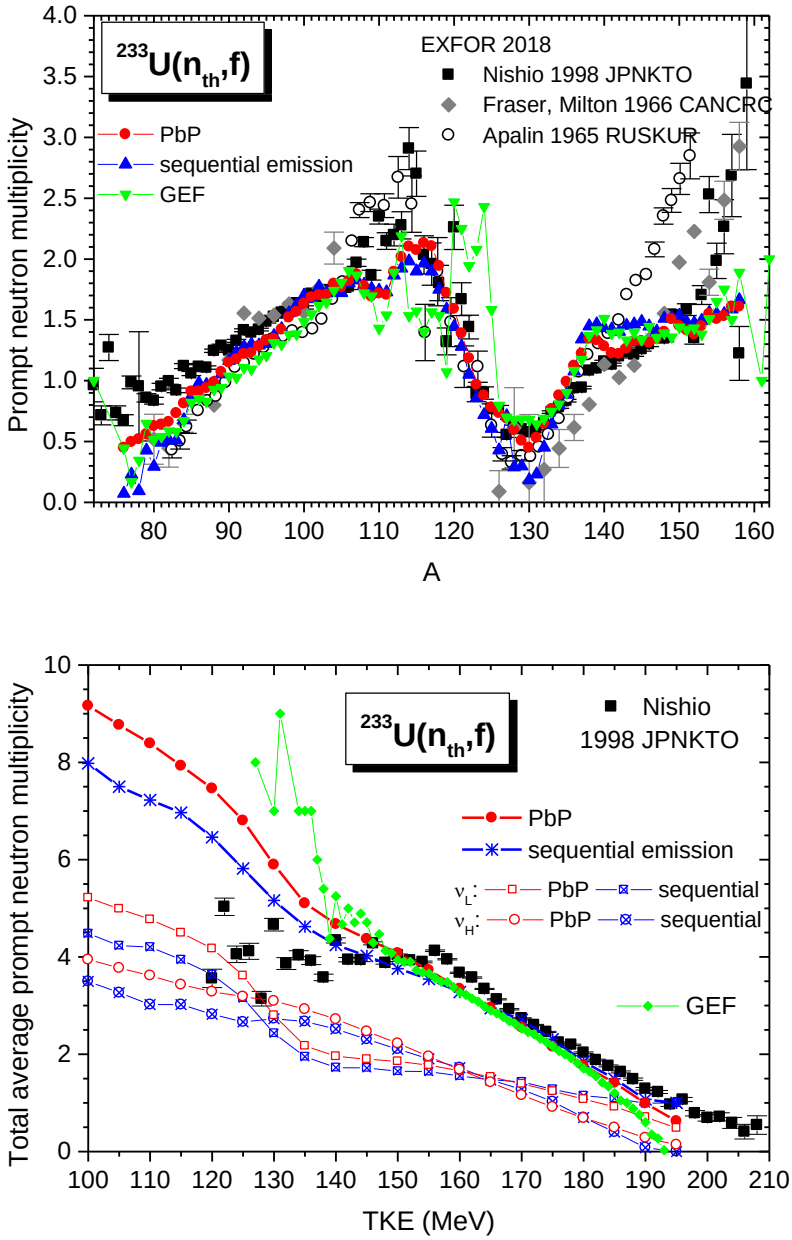

Fig.A3: Comparison of PbP (red symbols) and sequential emission (blue symbols) results of ν(A) (upper part) and ν(TKE) (lower part) with the results of GEF (green symbols) and the experimental data (different black and gray symbols).

As it can be seen both ν(A) and ν(TKE) of GEF are in overall agreement with the results of PbP and sequential emission modelings.

The ν(A) of GEF exhibit a very pronounced staggering at A symmetric fragmentation which is due to the limited number of 10^5 events used in the GEF calculation. The ν(A) of GEF is close to the sequential emission result over almost the entire A range, except at A around 130 where it exhibits a less pronounced minimum.

The ν(TKE) result of GEF is very close to the results of PbP and sequential emission models at TKE values ranging from 150 to 185 MeV.

The charge polarization ΔZ(A) and the root-mean-square of the isobaric charge distribution rms(A) provided by the GEF code are plotted in **Fig.A4** with green symbols in comparison with the results of the Zp model of [Wahl, 1988] (blue symbols) which were used in this work.

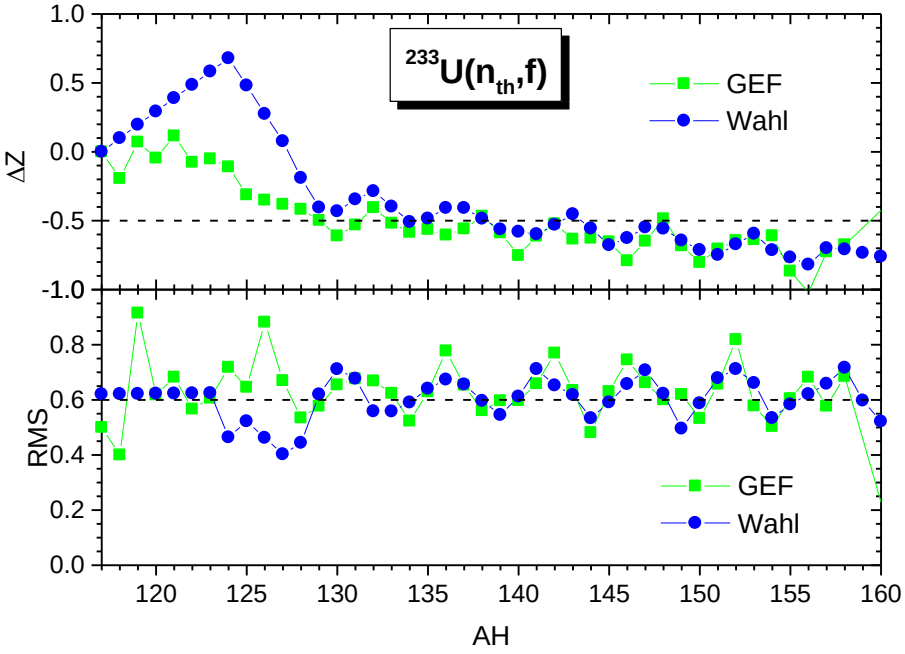

Fig.A4: ΔZ(A) (upper part) and rms(A) (lower part) of ^{233}U(n$_{th}$,f) provided by the GEF code (green symbols) and the Zp model of Wahl (blue symbols).

As it can be seen, ΔZ(A) and rms(A) of GEF are in agreement with those of the Zp model [Wahl, 1988] which were used in the prompt emission calculations of this work. In the asymmetric fission region both results of GEF and Zp model exhibit the well-known oscillations with a periodicity of about 5 mass units and they oscillate in phase. The oscillation amplitudes are a little bit higher in the case of GEF results.

The fragment mass distribution of ^{233}U(n$_{th}$,f) provided by the GEF code is plotted in **Fig.A5** with green diamonds, in comparison with the experimental Y(A) data of Surin (full red circles) and Nishio (blue squares with a cross inside). Differences between Y(A) of GEF and the experimental distributions are visible. Moreover the Y(A) result of GEF exhibits a pronounced staggering which means a higher even-odd effect compared to experimental data.

A part of total average quantities obtained in this work are in agreement with those provided by the GEF code. This is the case of energy release, i.e. $\langle Q \rangle_{GEF}$ = 187.791 MeV compared to $\langle Q \rangle_{PbP}$ = 187.553 MeV and of total kinetic energy of initial fragments at full acceleration $\langle TKE \rangle_{GEF}$ = 171.176 MeV compared to $\langle TKE \rangle_{PbP}$ = 171.902 MeV.

Note, the visible differences between Y(A) of GEF and Surin (which was used in this work) are expected to be reflected in differences between different total average quantities provided by GEF and those of this work.

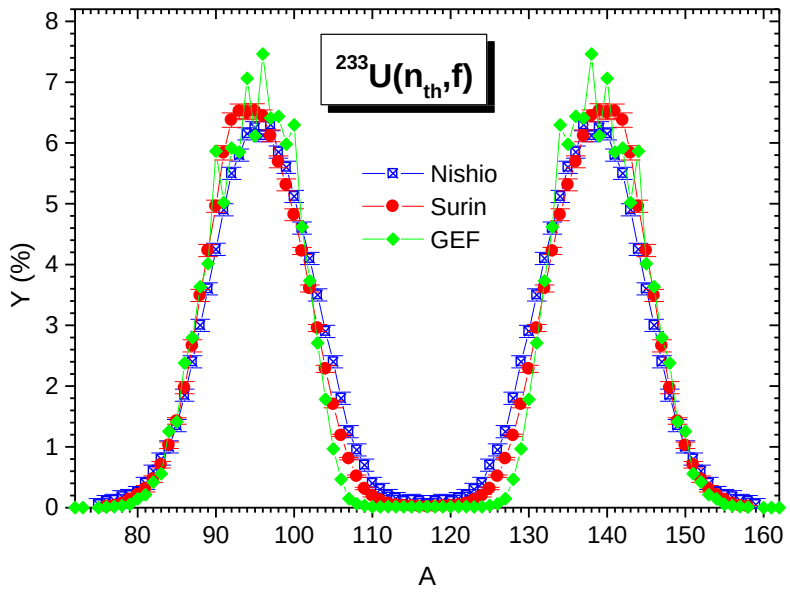

Fig.A5: Y(A) of $^{233}U(n_{th},f)$ provided by the GEF code (green diamonds) in comparison with the experimental data of Surin (full red circles) and Nishio (blue squares with a cross inside).

Consequently the total average prompt neutron multiplicity provided by GEF $\langle\nu\rangle_{GEF}$ = 2.424 is significantly lower than our result $\langle\nu\rangle_{PbP}$ = 2.481 which is in good agreement with the experimental data and the recent evaluations ENDF/B-VIII (<ν>=2.479), JEFF3.3 (<ν>=2.489) and JENDL4 (<ν>=2.478).

The total average prompt γ-ray energy and multiplicity provided by the GEF code differ significantly from the experimental data of Pleasonton and the results of PbP and sequential emission modelings as it can be seen in the table below:

Table A1<Eγ> and <Nγ> provided by the PbP and sequential emission modelings and by the GEF code in comparison with experimental data.

	<Eγ> (MeV)	<Nγ>
Pleasonton (exp)	6.69 ± 0.3	6.31 ± 0.3
PbP	6.581	6.197
Sequential emission	6.480	6.577
GEF	7.429	6.804

In other words, the total average prompt neutron multiplicity provided by the GEF code underestimate all experimental data and the recent evaluations as well as the present PbP and sequential emission results. The <Eγ> and <Nγ> results of GEF overestimate the experimental data of Pleasonton and the present results of PbP and sequential emission models.

References

Al-Adili, A., (2013). Measurements of the 234U(n,f) reaction with a Frisch-Grid ionization chamber up to En=5 MeV, PhD Thesis, Uppsala University, Sweden.

Bersillon, O., (2010), SCAT2 optical model code. NEA-Data Bank, Computer Program Service, Package NEA 0829/07 version 2010 (V.Manea, University of Bucharest) http://www.oecd-nea.fr/databank/.

Capote R. Noy (Ed), (2013), IAEA Headquarters, 13–16 December 2011, Summary Report INDC(NDS)-0608 IAEA, Vienna, Austria.

Capote R., Chen Y.-J., Hambsch F.-J., Kornilov N. V., Lestone J. P., Litaize O., Morillon B., Neudecker D., Oberstedt S., Ohsawa T., Otuka N., Pronyaev V. G., Saxena A., Serot O., Shcherbakov O. A., Shu N.-C., Smith D. L., Talou P., Trkov A., Tudora A., Vogt R., and Vorobyev A. S., (2016*) Nucl. Data Sheets* 131, 1-106.

EXFOR Experimental Nuclear Data Library (available online https://www-nds.iaea.org), target U-233, reaction (n,f), entries 40112004 (Y(A)), 40112007 (TKE(A)), 21771014 (TKE(A), σ_{TKE}(A)).

EXFOR Experimental Nuclear Data Library (available online https://www-nds.iaea.org), target U-233, reaction (n,f), quantity MFQ, data of Nishio (entries 22660005, 22660007, 22660008), Apalin (entry 41397004), Fraser and Milton (entry 14369004).

Fréhaut J., (1989) in IAEA-INDC(NDS)-220.

Gatera A., Göök A., Hambsch F.-J., Moens A., Oberstedt A., Oberstedt S., Sibbens G., Vanleeuw D., Vidali M., (2018), *EPJ Web of Conferences 169*, 00003.

Gook A., Hambsch F.-J., Vidali M.,(2014), *Phys. Rev. C* 90, 064611.

Gook A., Hambsch F.-J., Oberstedt S., (2017), *in THEORY-4 Scientific Workshop on Nuclear Fission Dynamics and the Emission of Prompt Neutrons and Gamma Rays, 20–22 June 2017*, Varna, Bulgaria, to be published in EPJ Web of Conferences.

Kawano T., Talou P., Chadwick M. B., Watanabe T., (2010), J.Nucl. Sci. Tech. 47, 462.1.

Litaize O., Serot O., (2010),*Phys. Rev. C* 82, 054616.

Madland D.G., Nix R., (1982), *Nuclear Science and Engineering*, 81, 213-271.

Madland D.G., (2006), *Nucl. Phys. A* 772, 113.

Madland D.G., Kahler A.C., (2017), *Nucl. Phys. A* 957, 289–311.

Marten H., Ruben A., Seelinger D., (1989), *IAEA-INDC(NDS)* ***220***, 47-57

Morariu C., Tudora A., Hambsch F.-H., Oberstedt S., Manailescu C., (2012), *J. Phys. G:Nucl. Part. Phys.* **39**, 055103

Nifenecker H.(1973), IAEA-SM-174/207, 117 review paper.

Oberstedt A., Billnert R., Gatera A. , Göök A., Oberstedt S.,(2018), EPJ Web of Conferences 169, 00014.

Ohsawa T. in Report INDC (NDS)-0608, pp. 23–26 of Ref. (Capote et. al., 2013).

Physics Simulation Packages: nuclear.llnl.gov/simulation/main.html.

Pleasonton F., (1973), Nucl. Phys. A 213, 413-425.

Qi L., Wilson J.N., Lebois M., Al-Adili A. , Chatillon A. , Choudhury D. , Gatera A. , Georgiev G., Göök A., Laurent B., Maj A., Matea I., Oberstedt A., Oberstedt S., Rose S.J., Schmitt C., Wasilewska B., Zeiser F. (2018) EPJ Web of Conferences 169, 00018.

Regnier D., Litaize O., Serot, O., (2013), Phys. Procedia 47, 47–52.

RIPL-3 Reference Input Parameter Library (2009a) of IAEA, segment I "Nuclear masses and deformations", database of Möller and Nix. Available online at https://www-nds.iaea.org.

RIPL-3 Reference Input Parameter Library (2009b), Segment 1 "Nuclear masses and deformations", data base of Möller and Nix (FRDM). Segment 5 "Nuclear densities"/ Shell correction prescription, database of shell corrections calculated with the Myers- Swiatecki mass formula.
Available online http://www-nds.iaea.org.

RIPL-3 Reference Input Parameter Library (2009c) of IAEA, segment IV "Optical model parameters", Becchetti-Greenlees. Available online at https://www-nds.iaea.org.

Ruben A., Marten H., Seelinger D., (1991), *Z. Phys. A***338**, 67-74

Schmidt K.-H., Jurado B. , Amouroux C., Schmitt C., (2016), Nucl.Data Sheets 131, 107-221.

Talou P., Becker B., Kawano T., Chadwick M. B., Danon Y., (2011), Phys. Rev. C 83, 064612.

Tudora, A., Vladuca, G., Morillon, B., (2004), Nucl. Phys. A 740, 33–58.

Tudora A., (2009), Annals of Nuclear Energy 36, 72–84.

Tudora A., Hambsch F.-J., Giubega G., Visan I., (2015a), Nucl. Phys. A 933, 165–188.

Tudora A., Hambsch F.-J., Visan I., Giubega G., (2015b), Nucl. Phys. A 940, 242–263.

Tudora A., Hambsch F.-J., Oberstedt S., Giubega G Visan I. (2015c), Nuclear Science and Engineering, 181:3, 289-301.

Tudora A., Hambsch F.-J., (2017), Eur. Phys. J. A. 53, 159.

Tudora A., HambschF.-J., (2018), EPJ Web of Conferences 169, 00025.

Tudora A., HambschF.-J., Tobosaru V., (2018), Eur. Phys. J. A. 54, 87.

Vladuca, G., Tudora, A., 2001a. Ann. Nucl. Energy 28, 419–435.

Vladuca, G., Tudora, A., 2001b. Ann.Nucl.Energy 28, 689–700.

Vladuca, G., Tudora, A., 2001c. Ann. Nucl. Energy 28, 1653–1665.

Vogt R., Randrup J., (2014), Phys.Rev. C 90, 064623.

Wahl A.C., (1988) Atomic Data and Nuclear Data Tables 39, 1-156.